AD-A136 328 EFFECTS OF VARIATIONS IN HEAT TREATMENT ON THE MECHANICAL PROPERTIES AND.. (U) NATIONAL BUREAU OF STANDARDS BOULDER CO FRACTURE AND DEFORMAT..

1/1

UNCLASSIFIED G E HITCHO ET AL. MAY 83 F/G 11/6 NL

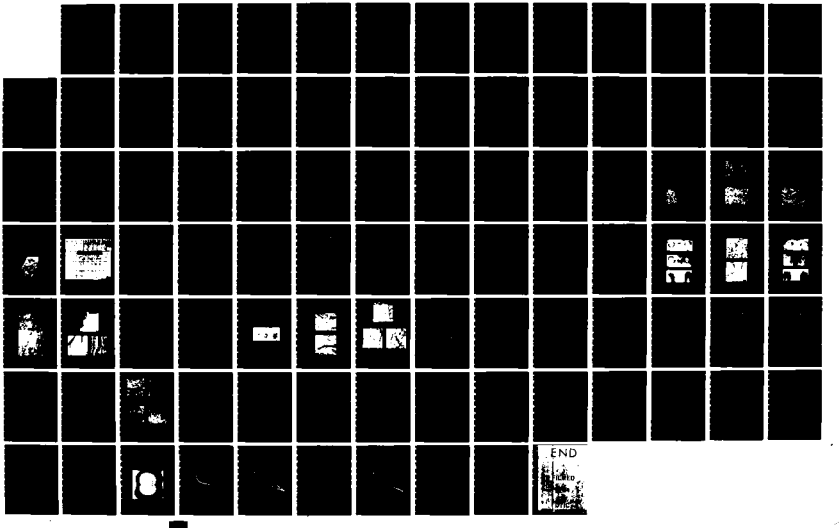

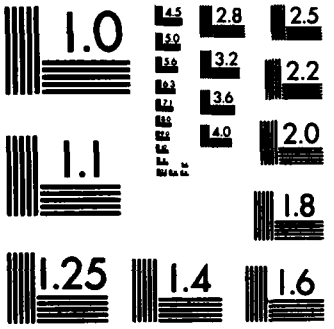

MICROCOPY RESOLUTION TEST CHART
NATIONAL BUREAU OF STANDARDS-1963-A

DTNSRDC-SME-CR-22-83

Contract No. N00167-82-MP-00032

EFFECTS OF VARIATIONS IN HEAT TREATMENT ON THE MECHANICAL PROPERTIES AND MICROSTRUCTURE OF ASTM A710 GRADE A CLASS 3 STEEL

by

G. E. Hitcho
L. C. Smith
S. Singhal
R. J. Fields

U.S. Department of Commerce
National Bureau of Standards
Fracture and Deformation Division
Washington, DC 20234

May 1983

Prepared for

David W. Taylor Naval Ship R&D Center
Annapolis, Maryland 21402

UNCLASSIFIED

SECURITY CLASSIFICATION OF THIS PAGE (When Data Entered)

REPORT DOCUMENTATION PAGE	READ INSTRUCTIONS BEFORE COMPLETING FORM
1. REPORT NUMBER: DTNSRDC/SME-CR-22-83	2. GOVT ACCESSION NO.: AD-A135 324
	3. RECIPIENT'S CATALOG NUMBER
4. TITLE (and Subtitle): EFFECTS OF VARIATIONS IN HEAT TREATMENT ON THE MECHANICAL PROPERTIES AND MICROSTRUCTURE OF ASTM A710 GRADE A CLASS 3 STEEL	5. TYPE OF REPORT & PERIOD COVERED: Research & Development
	6. PERFORMING ORG. REPORT NUMBER
7. AUTHOR(s): G. E. Hitcho, L. C. Smith, S. Singhal, and R. J. Fields	8. CONTRACT OR GRANT NUMBER(s): N000167-82-MP-00032
9. PERFORMING ORGANIZATION NAME AND ADDRESS: U.S. Department of Commerce, National Bureau of Standards, Washington, DC 20234	10. PROGRAM ELEMENT, PROJECT, TASK AREA & WORK UNIT NUMBERS: Program Element 62761N, Task Area SF-61-541-591, Work Unit 2803-132
11. CONTROLLING OFFICE NAME AND ADDRESS: Naval Sea Systems Command (SEA 05R25), Washington, DC 20362	12. REPORT DATE: May 1983
	13. NUMBER OF PAGES
14. MONITORING AGENCY NAME & ADDRESS (if different from Controlling Office): David W. Taylor Naval Ship R&D Center (Code 2814), Bethesda, MD 20084	15. SECURITY CLASS. (of this report): UNCLASSIFIED
	15a. DECLASSIFICATION/DOWNGRADING SCHEDULE

16. DISTRIBUTION STATEMENT (of this Report)

APPROVED FOR PUBLIC RELEASE; DISTRIBUTION UNLIMITED.

17. DISTRIBUTION STATEMENT (of the abstract entered in Block 20, if different from Report)

18. SUPPLEMENTARY NOTES

19. KEY WORDS (Continue on reverse side if necessary and identify by block number)

Age hardening steel
Cleavage fracture
Ductile fracture
Energy absorbed
Lower yield strength
Microstructure
Precipitate
Ultimate Tensile Strength
Upper yield strength

20. ABSTRACT (Continue on reverse side if necessary and identify by block number)

A final report assessing the effects of variations in heat treatment on the mechanical properties and microstructure of ASTM A710 grade A class 3 steel is given. The goal of this project was to evaluate the sensitivity of the mechanical properties of A710, an age hardening steel, to heat treatment variations that may occur in the production of thick plate.

(Continued on reverse side)

DD FORM 1 JAN 73 1473 EDITION OF 1 NOV 65 IS OBSOLETE S/N 0102-014-6601

UNCLASSIFIED

SECURITY CLASSIFICATION OF THIS PAGE (When Data Entered)

Block 20 continued

Tensile and impact tests were conducted on the material heat treated under the various conditions. Microstructure evaluations using optical and electron metallographic methods were conducted. Small angle neutron scattering examinations were also performed on selected specimens in order to evaluate the precipitate distribution. Results indicate that austenitization and aging time has little effect on the resultant mechanical properties. However, the mechanical properties were found to be sensitive to aging temperature. Impact results at $0^{\circ}F$ indicate that aging at $900^{\circ}F$ is detrimental in that the fracture surfaces of the broken impacts exhibited cleavage. Furthermore, the results suggest that welding or similar heating operations will not seriously degrade this material's properties.

EFFECTS OF VARIATIONS IN HEAT TREATMENT ON THE MECHANICAL PROPERTIES AND MICROSTRUCTURE OF ASTM A710 GRADE A CLASS 3 STEEL

by

G. E. Hitcho
L. C. Smith
S. Singhal
R. J. Fields

U.S. Department of Commerce
National Bureau of Standards
Fracture and Deformation Division
Washington, DC 20234

May 1983

Prepared for the David Taylor Naval Ship R&D Center
Contract N00167-82-MP-00032
Report Number DTNSRDC-SME-CR-22-83

A-1

TABLE OF CONTENTS

APPENDIX A - SMALL ANGLE NEUTRON SCATTERING (SANS) STUDY OF AGING OF ASTM A710 GRADE A, CLASS 3 STEEL

INITIAL DISTRIBUTION

LIST OF TABLES

LIST OF FIGURES

LIST OF FIGURES (Continued)

LIST OF FIGURES (Continued)

Effects of Variations in Heat Treatment on the Mechanical Properties and Microstructure of an ASTM A710 Grade A Class 3 Steel

G.E. Hicho*, L.C. Smith*, S. Singhal+, and R.J. Fields*

National Bureau of Standards
Washington DC 20234

A final report assessing the effects of variations in heat treatment on the mechanical properties and microstructure of ASTM A710 grade A class 3 steel is given. The goal of this project was to evaluate the sensitivity of the mechanical properties of A710, an age hardening steel, to heat treatment variations that may occur in the production of thick plate. Tensile and impact tests were conducted on the material heat treated under the various conditions. Microstructure evaluations using optical and electron metallographic methods were conducted. Small angle neutron scattering examinations were also performed on selected specimens in order to evaluate the precipitate distribution. Results indicate that austenitization and aging time has little effect on the resultant mechanical properties. However, the mechanical properties were found to be sensitive to aging temperature. Impact results at 0°F indicate that aging at 900°F is detrimental in that the fracture surfaces of the broken impacts exhibited cleavage. Furthermore, the results suggest that welding or similar heating operations will not seriously degrade this material's properties.

Key Words: age hardening steel, cleavage fracture, ductile fracture, energy absorbed, lower yield strength, microstructure, precipitate, ultimate tensile strength, upper yield strength.

*Fracture and Deformation Division, Center for Materials Science, National Measurement Laboratory
+Reactor Division, Center for Materials Science, National Measurement Laboratory

ADMINISTRATIVE INFORMATION

The investigation reported herein was funded by the Submarine Materials Block Program sponsored by Dr. H. H. Vanderveldt, Naval Sea Systems Command (SEA 05R25), and funded under Program Element 62761N, Task Area SF-61-541-591, Work Unit 2803-132. The effort was monitored by Mr. E. J. Czyryca, David Taylor Naval Ship R&D Center (Code 2814). This report satisfied in part Milestone PS 3.1/2 of Submarine Block Task, "Development of Thick-Plate HSLA Steels for Naval Applications", which is supervised by Mr. J. P. Gudas, David Taylor Naval Ship R&D Center (Code 2814).

INTRODUCTION

This report presents data as to whether temperature and time variations in the recommended heat treatment have any effect on the mechcnical properties and microstructure of ASTM A710 grade A, class 3 steel. The recommended heat treatment requires the steel to be austenitized at 1650°F for 68 minutes, water quenched, and aged at 1100°F for 30 minutes followed by air cooling.

In this report, results will be shown which compare the mechanical properties obtained after short (30 minute) and long (90 minute) austenitzation times at 1650°F, followed by aging times of 30,60, and 90 minutes at temperatures of 900, 1000, 1100, and 1200°F.

The steel, is an age-hardening ferritic steel containing about 1.2 weight percent copper. The copper is the primary strengthening element. Basically, the strengthening mechanism is as follows. During a soaking period at the austenitization temperature, a certain amount of copper goes into solid solution. When the steel is water quenched, the copper is retained in a supersaturated solid-solution. Subsequent aging of the steel at a selected temperature and time allows fine copper-rich precipitates to form within the ferrite. These precipitates impede dislocation motion, hence controlling the yield strength of the steel. In the as-quenched condition, the yield strength is about 60KSI. By aging this steel at 1100°F for 30 minutes, the recommended treatment, the yield strength is increased to 80-90KSI. In addition to the strengthening brought about by the precipitation of the fine copper phase, further strengthening is obtained by the addition of Cb. Columbium, when added to the melt, enhances grain refinement in the steel. This addition tends to lower the γ-α transformation, thereby enhancing nucleation, and at the same time retarding the growth of ferrite. This leads to a very fine ferrite grain size. Because precipitation hardening is the primary

strengthening mechanism, the melt carbon content can be low, thereby promoting good weldability, while retaining good ductility and strength. Since copper is one of the primary alloying elements in this steel, it is quite possible that hot shortness could be a problem. To eliminate this problem, nickel is added to the steel (1). Small amounts of Cr and Mo are also added to retard auto-aging which might occur after hot rolling. The combination of low carbon, strengthening by aging of the epsilon copper phase, and grain refinement appears to produce a steel with significantly improved strength and toughness qualities. (2) Jesseman et. al. and Hurley et. al. (3) have published papers showing the mechanical properties of the steel after austenitizing and aging at the recommended temperatures.

Optical examinations were conducted on the test coupons in order to obtain a correlation between microstructure and strength. Scanning electron microscopy (SEM) examinations were also conducted on the fracture surfaces of both the tensile and impact specimens. Small angle neutron scattering (SANS) studies were conducted on some samples as a function of aging time and temperature in order to evaluate both copper precipitate size and distribution. Correlations were found between the ultimate tensile, upper yield, lower yield, impact energy, and hardness. With these results, conclusions are drawn as to the sensitivity of A710 to variations in heat treatment.

AS RECEIVED PLATE

A plate of A710 steel, approximately 1 1/4 inch x 2 feet x 2 feet was used in the investigation. The mill report indicates that the plate was austenitized at 1650°F for 68 minutes and then water quenched. The

plate was subsequently aged hardened at 1100°F for 30 minutes and air cooled. The rolling direction was marked on the plate with paint.

Before test coupons were removed from the plate, a sample was removed and metallographically examined to verify the marked rolling direction. It was hoped that the inclusion shape and orientation would reveal the rolling direction. Figure 1 shows the unetched steel in the three orthogonal directions. The photomicrographs reveal the presence of globular sulfides indicating that inclusion shape control was used (usually by Ca addition to the melt). When low sulfur contents (.010 weight percent or less) are requested, Ca is added to the steel. Ca additions tend to globularize the sulfur in the steel and this dramatically improves the shelf energy of the steel. Because of the Ca addition, it was almost impossible to ascertain the plate's rolling direction, hence the direction marked on the plate was taken as the rolling direction. The chemical composition, as reported by the manufacturer is given in Table 1. Of note is the very low sulfur content (.004 weight percent).

MICROSTRUCTURE OF THE AS RECEIVED PLATE

The etched microstructures, in an orthogonal representation, are shown in Figure 2. The microstructure consists mainly of massive ferrite which, despite its name, is very fine grained. In the interior of the plate, there is evidence of some long range diffusional decomposition product. This is due probably to the fact that the interior of the plate can not be cooled as rapidly as its surface. Optical photomicrographs of the plate at higher magnification, Figures 3a, b, and 4a, b, show the presence of pearlite and possibly some bainite. The dull appearance of the ferrite could be due to the presence of an excessive amount of copper (4). It is

quite possible that some retained austenite is present, but this possibility was not investigated further.

The mill report stated that the grain size number was 8; however, our measurements found the grain size to be number 9.5 to 10. This finer grain size is not detrimental. Quite the contrary, the finer grain size enhances the mechanical properties of the steel.

A high resolution electron micrograph of A710 is shown in Figure 5. The dark particles are the incoherent FCC copper-rich precipitates. No finer precipitates were found. As noted by Hornbogen (5), there is no source of diffraction contrast for coherent copper precipitates in iron. For this reason, neutron scattering techniques were employed and are detailed in Appendix A.

SECTIONING OF THE TEST COUPONS FROM THE AS RECEIVED PLATE

The as-received plate was cut along the lines shown in Figure 6. Each test coupon was approximately 6 in. long, 2 1/2 in. wide and the thickness of the plate. From each coupon, two .500 in. diameter tensile specimens and three standard Charpy V-notch (CVN) specimens were prepared. The specimens were taken as close as possible to the quarter-thickness location in the plate. The tensile specimens were oriented with the longitudinal axis transverse to the rolling direction. The orientation of the CVN specimens corresponded to the ASTM TL direction; that is, the axis was transverse to the rolling direction of the plate and the notch located parallel to the rolling direction. It should be noted that each individual heat treatment was performed on each coupon prior to machining.

HEAT TREATING OF THE TEST COUPONS

The heat treatment schedule is shown in Table 2. Before heat treating each coupon, the time to reach the austenitization temperature of 1650°F, and

the times to reach the aging temperatures of 900°F, 1000°F, 1100°F, and 1200°F were determined. To accomplish this, thermocouples were inserted into selected coupons and temperature/time curves, Figure 7, for each condition were obtained. In addition, a thermocouple was also immersed into the quench medium in order to monitor the bath temperature which was maintained at 70°F.

PREPARATION OF TEST SPECIMENS

The specimens used for the tensile tests were .500 inch in diameter and dimensioned according to ASTM Specification A370-77,1 (unchanged through 1982). The Charpy V-notched specimens were prepared and tested according to ASTM Specification E23-82. The notches were placed in the specimen with a broaching tool for reproducability.

TEST CONDITIONS

The tensile specimens were tested at room temperature using a universal testing machine. Calibration data for the testing machine indicated that the accuracy of the load readings was within ±1% as recommended by ASTM Committee E-4 on testing. An extensometer was placed on the specimen to measure the percent strain over a 2 inch gage length. Figure 8 shows a typical stress/strain curve obtained for this material. ASTM specification A370-82 recommended the loading rate be 0.01in/in/min prior to yield, then 0.1in/in/min after yield for a specimen having a gage length of 2 inches.

The CVN specimens were tested at 0°F according to ASTM specification E23-82. They were immersed in the bath medium (ethyl alcohol) and held at temperature for at least 30 minutes before testing. The bath was magnetically stirred and the temperature was constantly monitored with a thermocouple.

TEST RESULTS (Summary Tables)

A summary of the test results (tensile, impact, and hardness) for the specimens austenitized at 1650°F for 30 minutes, water quenched, and aged at the appropiate temperatures and times are shown in Table 3. Similarly, results for specimens austenitized at 1650°F for 90 minutes, water quenched, and aged are shown in Table 4. In addition, tests were conducted on the as-received and the as-quenched plates. Specimens were also prepared after heat treating at the recommended austenitization temperature time of 1650°F for 68 minutes, and aged at 1100°F for 30, 60, and 90 minutes. These results are shown in Table 5.

TENSILE TEST RESULTS

In Figure 9, both the ultimate tensile stress (UTS) and lower yield stress (LYS)* increase when the material is aged for 30 minutes at 1000°F as compared to 900°F. This phenomenon was not found at aging times greater than 30 minutes. At temperatures greater than 1000°F, irregardless of aging time, both the UTS and LYS decrease drastically. Elongation and reduction of area increase at temperatures above 1000°F because of internal metallurgical mechanisms. The absence of data for specimen aged at 1200°F was this specimen was inadvertantly aged at 1100°F.

The shape of the tensile data curves, Figure 10, for specimens austenitized at 1650°F for 90 minutes, water quenched, and then aged, appear to be quite similar to these shown in Figure 9. Again there is an increase in the UTS and LYS as the aging temperature is increased from 900°F to 1000°F and, like the specimens austenitized for 30 minutes the UTS and LYS both decrease as the aging temperature increases. Elongation and the reduction of

*The LYS is equivalent to the 0.2% offset yield stress.

area also follow the trend established before - both increase as the aging temperature increases.

HARDNESS TEST RESULTS

Hardness results are shown in Tables 3, 4, and 5. Six Rockwell A measurements readings were taken on each impact specimen before testing. These values were then converted to the approximately equivalent Rockwell B values for presentation in the tables.

Figure 11 shows hardness plotted as a function of precipitation hardening time. Hardness decreases as both the aging time and temperature increase. One exception to that trend occurs at the aging temperature of 900°F, regardless of austenitizion time. At that aging temperature, the hardness increases significantly after aging times of 60 and 90 minutes. This indicates that the A710 is underaged at 900°F and overaged at all higher temperatures including the temperature of the manufacturer's recommended treatment. Further heating of overaged material, such as might occur in the heat affected zone (HAZ), will only slightly decrease the hardness.

These results are more clearly shown in Figures 12 and 13 where hardness, HRB is shown as a function of precipitation hardening temperature. It is shown that at aging temperatures greater than 900°F, the hardness obtained with longer aging times and higher temperatures is always lower that obtained with shorter aging times and lower temperatures. At 900°F, however, the hardness obtained after aging times of 60 and 90 minute was greater than that obtained after 30 minutes. This appears to be due to the thermodynamics associated with the epsilon-copper phase formation. Previous work on Fe-0.9% Cu (5) has shown that after short aging times of 2, 8, or 10 minutes, at 900°F, hardness is still increasing, whereas for the same aging times, at 1000°F, the hardness has leveled off. It appears from the hardness data for

the A710 that at the aging temperature of 900°F, the maximum hardness has not yet been achieved, even for the aging time of 90 minutes.

The curves in Figures 12 and 13 are quite similar to the strength versus precipitation hardening temperature curves shown in Figures 10 and 11. Like the strength curves, the highest hardness was obtained at the aging temperature of 900°F and aging time of 90 minutes.

IMPACT TEST RESULTS

Charpy V-notch impact test results for specimens tested at 0°F are shown in Tables 3 and 4 and Figures 14 and 15. The energy absorbed values are the lowest after aging at 900°F, regardless of austenitization time. As the aging temperature increases, so does the energy absorbed. An anomaly is observed for the specimen austenitized for 90 minutes and then aged for 30 minutes at 1000°F. The energy absorbed is essentially the same as that obtained at an aging time of 30 min at 900°F. The reason for this is unknown at this writing. Comparison of Figures 14 and 15 indicates that there is more scatter in the data for the material austenitized for 90 minutes.

Table 6 shows the results of the energy absorbed values obtained for both austenitizing times and at the various aging temperatures. The 900°F treatment, which is shown to result in low impact properties, corresponded to the highest UTS and LYS values. It can also be seen that overaging results in improved impact resistance. This has good implication with regard to weld heat affected zone toughness. That is, further heating will only toughen the material. From these impact results, it can be concluded that the austenitization time has no significant effect on impact properties.

FRACTOGRAPHIC EXAMINATION RESULTS

A. Tensile Specimens

Photographs, taken at low and high magnifications of selected broken tensile specimens, are shown in Figures 16 and 17.

Figure 16 shows the normal cup and cone type fracture. Corresponding scanning electron micrographs, Figure 17, taken at a higher magnification, show fracture surfaces characteristic of a ductile material - voids that have coalesced and subsequently fractured.

Upon examination of other fractured tensile specimens, splitting in the fracture surface was observed. Some of the specimens that showed splitting are shown in Figure 18. Splits in the material were found parallel to the loading direction. A higher magnification observation using the SEM, Figure 19, taken along the split, was unable to clearly identify the fracture characteristics of the split.

In another SEM examination of a specimen that was severely split, Figure 20a, b, and c, it was observed that the fracture was predominately ductile in nature as evidenced by the shear observed on the fracture surface. No further conclusions could be drawn as to the cause of the splitting; however, it was suggested that possible causes could have been stress induced hardening, an orientation effect, or possibly temper embrittlement. We feel, however, that splitting could be a stress state problem since two identically heat treated specimens responded differently when tested. While the tensile specimen that was machined to a diameter of 0.500 inch showed splitting, one that was machined to 0.252 inch showed no splitting at all. This specimen showed cup and cone fracture. The specimen that split did not show any evidence of cleavage fracture when observed on the SEM.

Figures 21 and 22 are graphical representations of the type of fracture observed on the test specimens as a function of the austenitization time and precipitation hardening temperature.

The figures show that some degree of splitting was observed at aging temperatures of 900°F, 1000°F, and 1100°F. At the aging temperature of

1200°F, irregardless of aging time, there was no evidence of splitting observed in the tensile specimens. Also at an austenization time of 90 minutes followed by an aging temperature and time of 900°F, 30 minutes respectively, was there an absence of splitting. The length of the austenitization time does not appear to dictate whether the specimen splits on loading.

Even though this splitting phenomenon was observed in some tensile specimens, it should be realized that the splitting occurred at reductions of area near 76% and elongations of 26%, well into the plastic instability region of the steel.

B. Impact Specimens

The fracture surfaces of several impact specimens were examined using a light microscope. There was no evidence of splitting in these specimens. A low magnification photograph of several broken impact specimens is shown in Figure 23. SEM fractographs of the same surfaces are shown in Figure 24. The fracture appearance of these are definitely ductile in nature.

Impact specimens fractures corresponding to the tensile specimens that contained splits were examined in the SEM. Some of these specimens showed evidence of cleavage fracture, others did not. With these conflicting results, it was decided to examine all of the impact specimen fractures with the SEM in order to determine which ones exhibited cleavage fracture and which ones did not. A micrograph of a impact specimen that revealed cleavage fracture is shown in Figure 25a, b, and c.

Figures 26 and 27 show the energy absorbed versus precipitation hardening temperature for both austenitization times. Printed on these curves are the letters C and D. The letters C and D appearing in these figures correspond to the observed fracture appearance - C indicates cleavage fracture and D

ductile fracture. It was found that cleavage fracture was observed only on those impact specimens that were aged at 900°F. Again, austenitization time does not appear to affect whether the fracture was ductile or brittle in nature.

For those specimens that showed cleavage, the cleavage did not extend over the entire surface. It was located primarily in the vicinity of the hammer's impact. The remainder of the sample's fracture surface was ductile exhibiting dimpled rupture.

CORRELATIONS BETWEEN OBSERVED RESULTS

It was perceived that a correlation might exist among the mechanical property results obtained in this work. One such correlation was developed using a combination of the UTS, the LYS, and energy absorbed. Figure 28 is a plot of these data.

In this figure, it is obvious that the correlation is not linear. However, it is shown that with a known UTS or LYS, one can roughly estimate a corresponding energy absorbed. The curves in Figure 28 also reveal that impact properties improve as the UTS and LYS decrease. There is a rapid decrease in these tensile properties once the impact energy exceeds 170 ft-lb.

Figure 29 is a plot of hardness and corresponding UTS and LYS values. Again, a linear correlation was not found, but as in the previous correlation for UTS, LYS, and energy absorbed, one could for only those heat treatments studied, knowing the hardness determine with reasonable accuracy either the UTS or LYS.

Figure 30 is a plot of hardness versus energy absorbed. From this curve it is possible to determine the approximate impact value from the hardness data. These data may be used to determine the most impact sensitive region of a HAZ.

One noticeable tensile property characteristic of this material is that it exhibits a load drop on yielding. This was shown in Figure 8, a drawing of the typical stress/strain curve that was obtained. Of importance is the degree of load drop; that is, the difference between the upper and lower yield stress values. This is probably due to the pinning of mobile dislocations by the copper precipitates. An analysis of the load drop for the specimens tested follows.

Figures 31 and 32 are plots of the upper yield stress minus the lower yield stress vs aging temperature, for different austenitization times. It is shown in these figures that this difference is most pronounced for material that was aged at 1100°F for austenitizing at either 30 or 90 minutes.

Figures 33 and 34 show curves developed by plotting the ratios of UYS and LYS to UTS versus precipitation hardening tmeperature. The LYS/UTS ratio is essentially constant over the range of aging temperatures, whereas the UYS/UTS ratio is very sensitive to the aging temperature. This sensitivity most pronounced is again at the reported optimum aging temperature, 1100°F. At this temperature the UYS/UTS is almost 99% of the UTS. While this is not significant in displacement controlled situations, it may be relevant in load control. It should be noted that at the optimum aging temperature of 1100°F, the reduction of area and elongation were found to be 75% and 26% respectively.

SMALL ANGLE NEUTRON SCATTERING (SANS) RESULTS.

The SANS work is detailed in Appendix A. Results indicate that, at an austenitization time of 90 minutes and aging temperature of 900°F for 30 minutes, the volume fraction of the epsilon-copper precipitate was lower than that observed for the other heat treating conditions. However, the distribution of the precipitate was finer, with closer inter particle distances, which led to a high hardness. It was also shown that the volume fraction of the precipitate increases as the aging

temperature increases. Furthermore, the excellent correlation between hardness and the total neutron cross section for the isochronically aged samples demonstrates the power of this microstructural tool.

DISCUSSION

In this work, the sensitivity of the mechanical properties A710 Grade A, Class 3 steel, to variations in heat treatment were determined. In particular, tensile and impact properties were measured as a function of austenitzation time, and aging temperature and time.

A710 steel is a precipitation hardening steel, and the element which is primarily responsible for this hardening is copper. After the proper austenitization time and temperature, the yield strength can be raised from its solution heat treated value of 60KSI to a yield strength in the range of 80-90KSI. This steel, used in the optimum quenched and aged condition, exhibits a microstructure consisting mainly of massive ferrite, which despite its name is very fine grained. The small grain size of the steel is attributed to the Cb addition which forms a columbium-carbon-nitride Cb(C,N) that tends to suppress grain growth during austenitization. It also reduces the transformation temperature. The measured grain size was 9.5 to 10 for the plate tested.

An examination of the as-polished surface, in three orthogonal directions, revealed the presence of globular inclusions. This is an indication that Ca was added to the steel for the purpose of inclusion shape control. Inclusion shape control (Ca addition) improves the impact properties significantly, in particular the shelf energy.

Transmission electron microscopy studies of the received plate revealed large, > 200 Å incoherent, copper precipitates that are probably responsible

for the increase in the yield strength on aging. The coherent epsilon-copper precipitate was not resolved in the STEM because of its small scattering contrast for electrons and because of its lack of coherency strain.

A more detailed analysis at the precipitation behavior was carried out by a technique called small angle neutron scattering (SANS). It was demonstrated (appendix A) that SANS could be used to determine the distribution and size of the precipitates.

Following these examinations, as received 1 1/4" thick plate was sectioned into coupons and each coupon heat treated according to a pre-determined schedule. Tensile and impact specimens were sectioned from the 1/4 thickness location of the plate and subsequently tested.

Previous tensile test results clearly indicate that A710 steel is significantly affected by the aging time but not the austenitizing time. The tensile tests also revealed that A710 exhibits upper and lower yield points. The change from the UYS to the LYS is called yield drop. This yield drop is followed by Luders band propagation, which is in turn followed by work hardening until the ultimate strength is reached. The ductility as measured by the reduction of area and elongation in the tensile tests was about 75% and 26% respectively - both indicative of a very tough material.

Table 7 shows a comparison of the UTS, UYS, and LYS values shown in Figures 9 and 10. It was reported by the manufacturer that the optimum aging temperature was 1100°F. Test data for specimens aged at temperatures below 1000°F were not found. However, in our investigation, specimens were aged at 900°F and tested. It was found that the tensile properties obtained after aging times of 60 and 90 minutes were greater than those reported for the optimum aging temperature and time. These results appear to be due to the size of the epsilon-copper precipitate formed after the 90 minute aging time

at 900F. The size of the precipitate formed is so fine and dispersed throughout the ferrite that dislocation motion is severely retarded. This dislocation retardation leads to higher flow stresses. At 1200°F, the precipitates are no longer fine, but are coarse due to overaging. The resulting precipitates are no longer coherent with the matrix and dislocations motion is much less difficult. This is manifested in lower flow stresses.

The tensile results for the steel aged at various temperatures indicated that the maximum strength was obtained after age hardening at a temperature of 900F, the impact energy values for this same aging temperature, tested at 0°F were low. SEM observations of these fracture surfaces show some cleavage. At an aging temperature of 1000°F and above, it appears that the material has passed through an optimum and is in an overaged condition. This overaging is advisable because overaging improves the impact properties significantly. The 900°F aging treatment corresponds to the highest ultimate and yield strength value, but lowest impact toughness. Overaging results in improved impact resistance and has good implications in regard to the heat affected zone weld toughness.

Attempts were made to develop correlations among tensile test values, hardness, and impact results. The most significant relationships obtained were those relating the tensile test results (UTS, LYS, UYS) and hardness. Attempts were made to relate the observed metallurgical microstructure of the aged material with the obtained mechanical properties. However, as shown in Figure 35, the microstructure did not vary noticeable for different aging conditions, hence this approach was disregarded. Because of this

observation, SANS was chosen. SANS (appendix A) did prove to be a viable tool in quantifying the precipitate distribution as a function of aging time and temperature. However the precipitate was not defined.

Scanning electron microscopic work on the fractured test samples revealed that some of the tensile specimens showed splits on the fracture surface. The splitting was thought to be due to the stress state. This splitting could be accentuated if the tensile specimens were tested in the through thickness direction. No through thickness specimens were tested in this work. The impact specimens did not show any evidence of this splitting. A710 grade A, class 3 steel was found to be insensitive to austenitization time, but quite sensitive to aging time and temperature.

CONCLUSIONS

1. Variations of ±30 minutes in austenitizing time at 1650 °F have very little effect on mechanical properties.
2. Variations of ±100 °F and ±30 minutes in the manufacturer's recommended aging treatment do not seriously degrade mechanical properties.
3. Tensile ductility is virtually unaffected by any of the variations noted in 1 and 2 above.
4. Degraded mechanical properties can be restored by suitable reaustenitization and aging treatment.
5. Manufactured plate is normally in an overaged condition. Further heating of this material by welding or other operation should only increase impact resistance.
6. Underaging at 900 °F considerably reduces impact properties.
7. UYS can approach UTS for some conditions. This may have ramifications for load controlled situations.
8. Longitudinal splitting of tensile specimens and cleavage during impact can occur for certain conditions. This may have ramifications for thicker sections or welded structures.

REFERENCES

1. Hydrean, P.P., Kitchin A.L., and Schaller, F.W., "Hot Rolling and Heat Treatment of Ni-Cu-Cb(Nb) Steel," Met. Trans., Sept. 1971, 2, p. 2541.

2. Jesseman, R.J., and Murphy, G.J. "High Strength Precipitation Hardened Alloy Steel For Heavy Section Application," Presented at the 1977 Triple Engineering Shows and Conferences, Chicago, see. Oct. 26, 1977.

3. Hurley, J.L., and Shelton, C.H., "Age-Hardenable Nickel-Copper Steels", Metals Quarterly, May, 1956, p. 25.

4. Creswick, W.E., "Commercial Development of A Rimmed Low-Alloy Precipitation-Hardening High Strength Steel," British Iron and Steel Institute, Publication 104, 1967.

5. Hornbogen, E., "Aging and Plastic Deformation of an Fe-0.9% Cu Alloy", Trans. ASM, Vol. 57, 1964, p. 120.

Table 1. Chemical analyses* of as received plate.

Heat Number	55180
Grain Size	8

Element	Weight Percent
C	0.04
Mn	0.58
P	0.010
S	0.004
Si	0.30
Cr	0.68
Ni	0.87
Mo	0.19
Cu	1.20
Cb	0.046

* As reported by manufacturer.

Table 2. Heat treating schedules for test specimens.

Short Austenitizing Time			Long Austenitizing Time		
1650°F - 30min - W/Q			1650°F - 90min - W/Q		
Specimen Number	Aging Time(min)	Aging Temp °F	Specimen Number	Aging Time(min)	Aging Temp °F
1	30	900	13	30	900
2	30	1000	14	30	1000
3	30	1100	15	30	1100
4	30	1200	16	30	1200
5	60	900	17	60	900
6	60	1000	18	60	1000
7	60	1100	19	60	1100
8	60	1200	20	60	1200
9	90	900	21	90	900
10	90	1000	22	90	1000
11	90	1100	23	90	1100
12	90	1200	24	90	1200

Also:

1650F - 68 min - W/Q then

Specimen 25 30 min @ 1100°F
" 26 60 min @ 1100°F
" 27 90 min @ 1100°F

28 As quenched, no aging
29 As received.

Table 3. Mechanical property results for specimens austenitized at 1650°F for 30 minutes, water quenched and aged at the indicated temperatures and times. Impact specimens tested at 0°F.

Specimen Number	Aging Time (min)	Aging Temp°F	UTS[a] (KSI)	UYS[a] (KSI)	LYS[a,*] (KSI)	EL[a] (%in2")	RA[a] (%)	HARD[b] (HRB)	ENERGY[c] ABSORBED (Ft-lb)
1	30	900	109.2	99.1	96.1	25.9	73.9	98.5	128.7
2	30	1000	111.5	104.8	98.0	26.6	72.3	99.0	161.3
3	30	1100	97.8	95.6	86.3	27.3	76.8	95.3	178.3
4	30	1200	90.3	89.4	81.5	29.4	79.5	92.0	195.0
5	60	900	113.2	104.5	101.3	26.0	73.0	99.8	107.3
6	60	1000	109.2	101.4	95.7	25.9	72.8	98.6	155.0
7	60	1100	96.3	95.8	86.2	28.3	76.4	95.0	178.3
8	60	1200	89.3	87.3	80.3	29.5	79.1	91.6	189.3
9	90	900	114.3	102.4	100.4	25.9	72.5	HRC 23.4	88.3
10	90	1000	105.7	97.2	91.4	27.3	73.3	98.0	156.7
11	90	1100	94.5	92.5	84.3	28.2	77.8	94.4	185.7
12	90	1200		NOT	TESTED				

(a) Average of 2 values
(b) Average of 6 values
(c) Average of 3 values

* LYS is equivalent to 0.2% effect yield stress.

Table 4. Mechanical property results for specimens austenitized at 1650°F for 90 minutes, water quenched and aged at the indicated temperatures and times. Impact specimens tested at 0°F.

Specimen Number	Aging Time(min)	Aging Temp°F	UTS[a] (KSI)	UYS[a] (KSI)	LYS[a] (KSI)	EL[a] (%in2")	RA[a] (%)	HARD[b] (HRB)	ENERGY[c] ABSORBED (Ft-lb
13	30	900	109.2	101.0	96.4	24.9	74.5	98.7	129.7
14	30	1000	111.7	103.4	98.1	27.3	72.7	99.8	128.7
15	30	1100	97.9	95.4	87.4	27.8	76.8	95.6	178.0
16	30	1200	90.4	88.7	81.0	29.7	79.4	91.2	193.0
17	60	900	110.9	101.0	97.7	25.4	72.0	99.8	96.3
18	60	1000	109.0	103.7	96.8	25.2	71.4	98.3	168.3
19	60	1100	95.4	93.2	85.4	27.8	76.8	94.4	178.0
20	60	1200	88.2	87.2	78.9	28.9	78.5	90.4	213.7
21	90	900	115.4	107.9	103.7	25.8	71.8	HRC 23.2	89.3
22	90	1000	105.8	100.1	93.8	26.0	73.4	98.5	167.0
23	90	1100	94.7	93.6	84.9	28.8	74.5	93.8	183.7
24	90	1200	85.2	83.5	76.6	30.8	80.8	89.0	204.0

(a) Average of 2 values
(b) Average of 6 values
(c) Average of 3 values

* LYS is equivalent to 0.2% effect yield stress.

Table 5. Results for specimens austenitized at 1650°F for 68 minutes and then water quenched. Impact specimens tested at 0°F.

Specimen Number	Aging Time(min)	Aging Temp°F	UTS[a] (KSI)	UYS[a] (KSI)	LYS[a*] (KSI)	EL[a] (%in2")	RA[a] (%)	HARD[b] (HRB)	ENERGY[c] ABSORBED (Ft-Lb)
25	30	1100	99.4	98.3	89.3	28.3	75.3	95.5	184.0
26	60	1100	95.9	94.4	86.1	27.7	76.9	94.6	190.7
27	90	1100	92.3	89.8	82.8	28.7	77.8	92.6	189.7
28	As Quenched (No Aging)		98.9	57.5[d]		27.8	72.9	94.2	169.3
29	As Received		95.2	90.8	81.7	28.3	76.1	93.8	200.0
Mill Report Test			(1)97.6 (2)93.7	89.0[d] 87.2[d]		25.0 26.0			

(a) Averagy of 2 Values
(b) Average of 6 Values
(c) Average of 3 Values
(d) 0.2% offset

* LYS is equivalent to 0.2% effect yield stress.

Table 6. Comparison of Charpy V-notch impact test results for both austenitization times. Specimens tested at 0°F.

		1650°F - 30 min-W/Q	1650°F - 90 min-W/Q
Aging Time(min)	Aging Temp°F	Energy Absorbed* (Ft - Lb)	Energy Absorbed* (Ft - Lb)
30	900	128.7	129.7
30	1000	161.3	128.7
30	1100	178.3	178.0
30	1200	195.0	193.0
60	900	107.3	96.3
60	1000	155.0	168.3
60	1100	178.3	178.0
60	1200	189.3	213.7
90	900	88.3	89.3
90	1000	156.7	167.0
90	1100	185.7	183./
90	1200	(Not Tested)	204.0

Also 1650°F - 68 min. - W/Q

30	1100	184.0
60	1100	190.7
90	1100	189.7
As Quenched (No Aging)		169.3
As Received		200.0

*Average of 3 Values

Table 7. Comparison of UTS, UYS, and LYS results.

		1650°F - 30 min - W/Q			1650°F - 90 min - W/Q		
Aging Time(min)	Aging Temp°F	UTS (KSI)	UYS (KSI)	LYS* (KSI)	UTS (KSI)	UYS (KSI)	LYS* (KSI)
30	900	109.2	99.9	96.4	109.2	101.0	96.4
30	1000	111.5	104.8	98.0	111.7	103.4	98.1
30	1100	97.8	95.6	86.3	97.9	95.4	87.4
30	1200	90.3	89.4	81.5	90.4	88.7	81.0
60	900	113.2	104.5	101.3	110.9	101.0	97.7
60	1000	109.2	101.4	95.7	109.0	103.7	96.8
60	1100	96.3	95.8	86.2	95.4	93.2	85.4
60	1200	89.3	87.3	80.3	88.2	87.2	78.9
90	900	114.3	102.4	100.4	115.4	107.9	103.7
90	1000	105.7	97.2	91.4	105.8	100.1	93.8
90	1100	94.5	92.5	84.3	94.7	93.6	84.9
90	1200	(Not Tested)			85.2	83.5	76.6

* LYS equivalent to 0.2% offset yield stress.

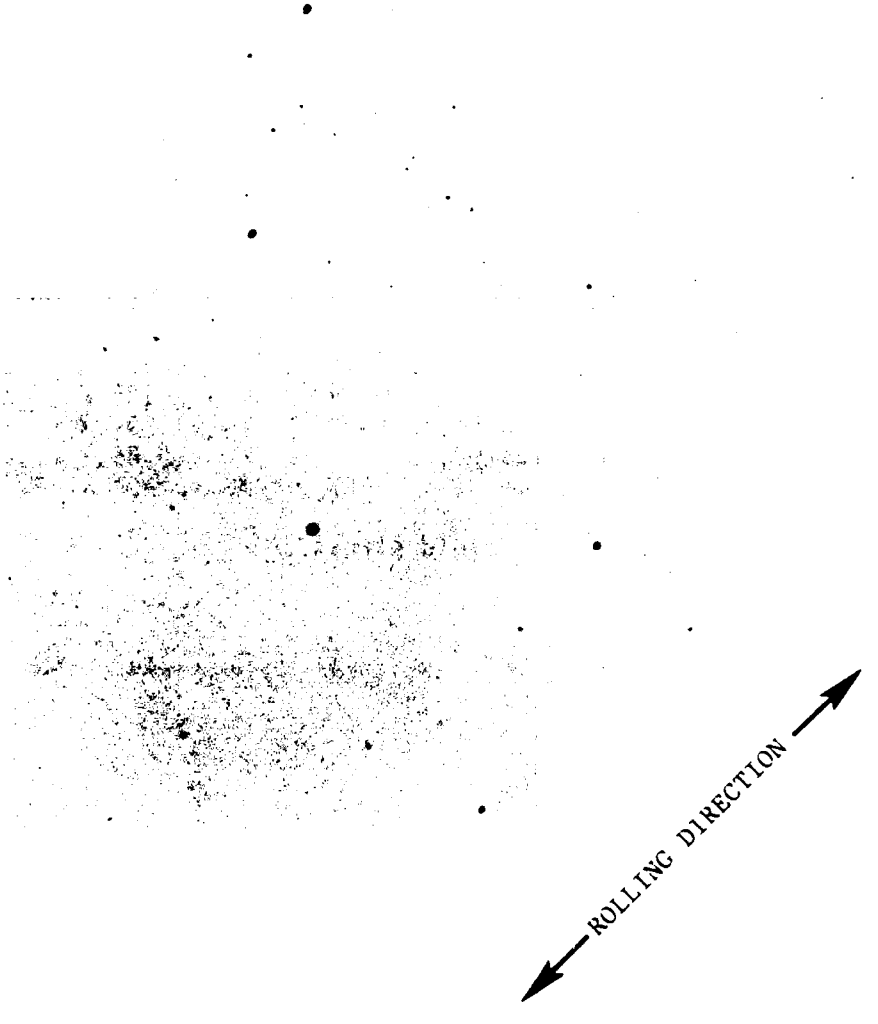

Figure 1. As received plate shown in the as polished condition. The orthogonal directions are shown. Magn. X100.

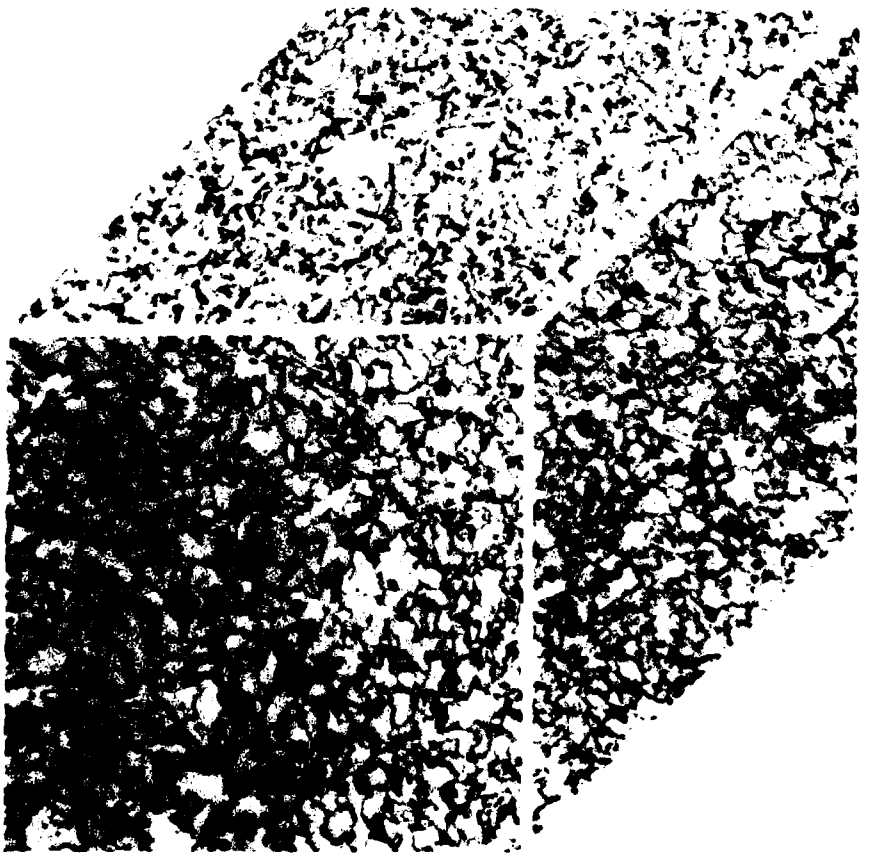

Figure 2. As received plate shown in the etched condition. The orthogonal directions are shown. Magn. X500 Etch: 1% Nital.

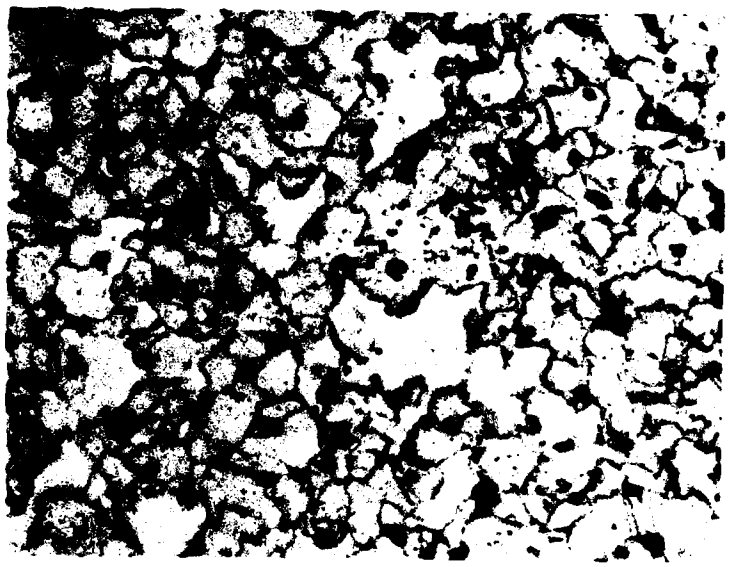

a.

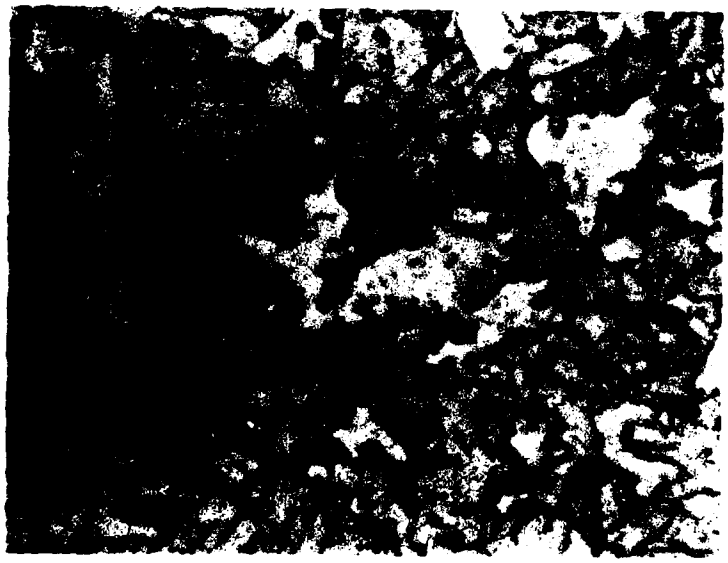

b

Figure 3. Microstructure of the as received plate at higher magnifications. Structure appears to be ferrite, bainite and some pearlite. (a) X500, (b) X1000 Etch: 1% Nital

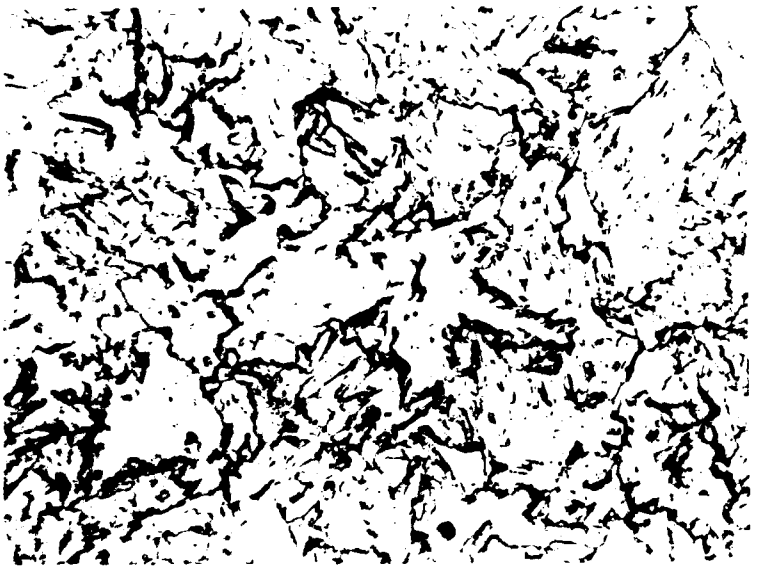

a

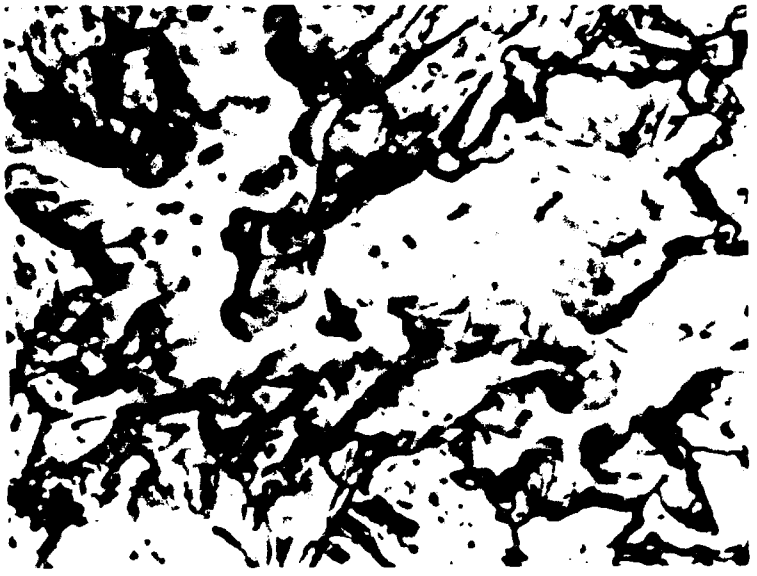

b

Figure 4. Microstructure of the plate's surface at higher magnifications. The dull appearance within the ferrite could possibly be due to the presence of the copper precipitate. (a) X1000, (b) X2500 Etch: 1% Nital

Figure 5. A high resolution transmission election microscopy photograph, STEM, of A710. The dark particles are incoherent FCC copper precipitates. X60000.

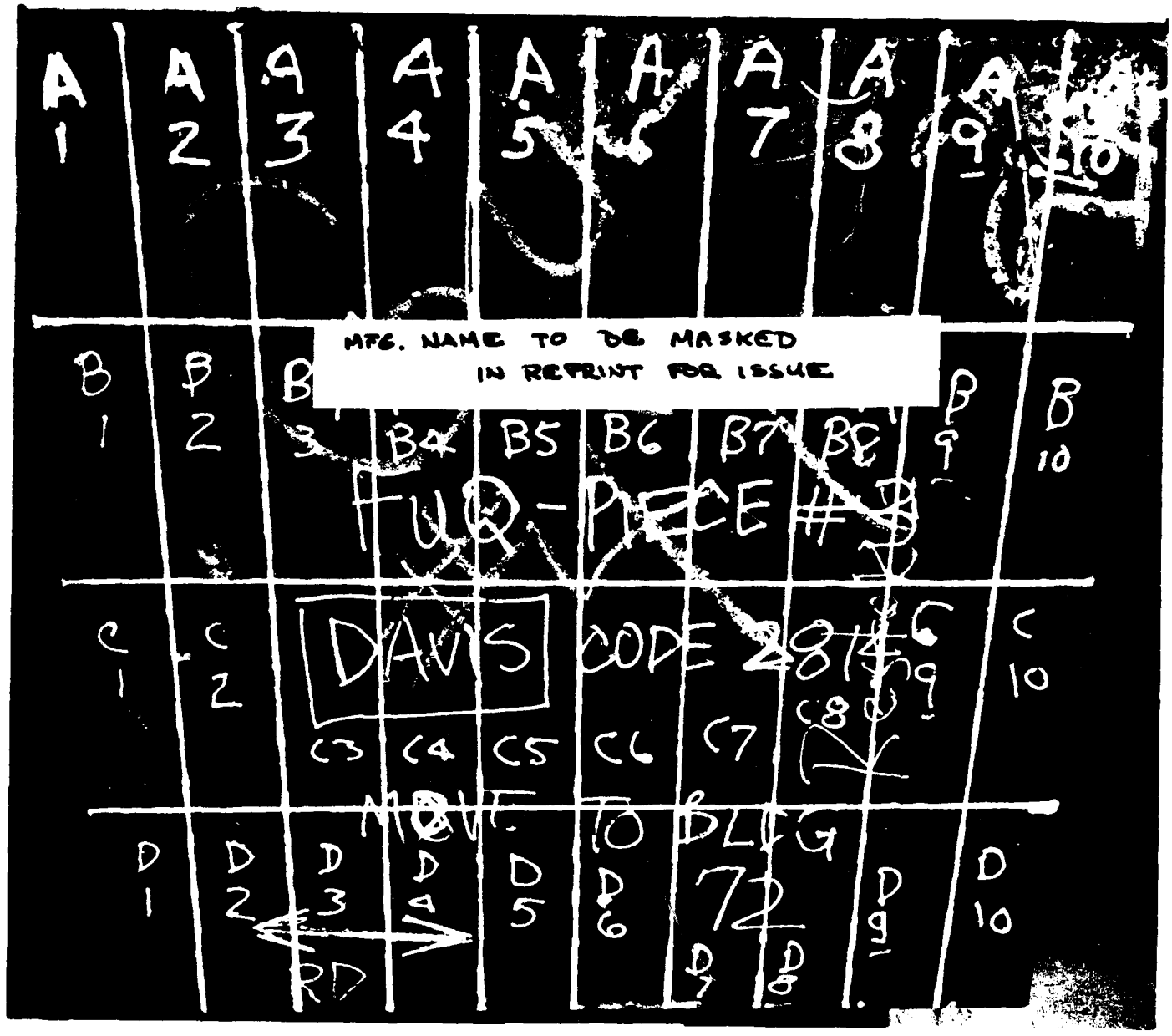

Figure 6. Photograph showing the location of each test coupon and the lines along which each was sectioned. Plate's rolling direction is indicated by arrow.

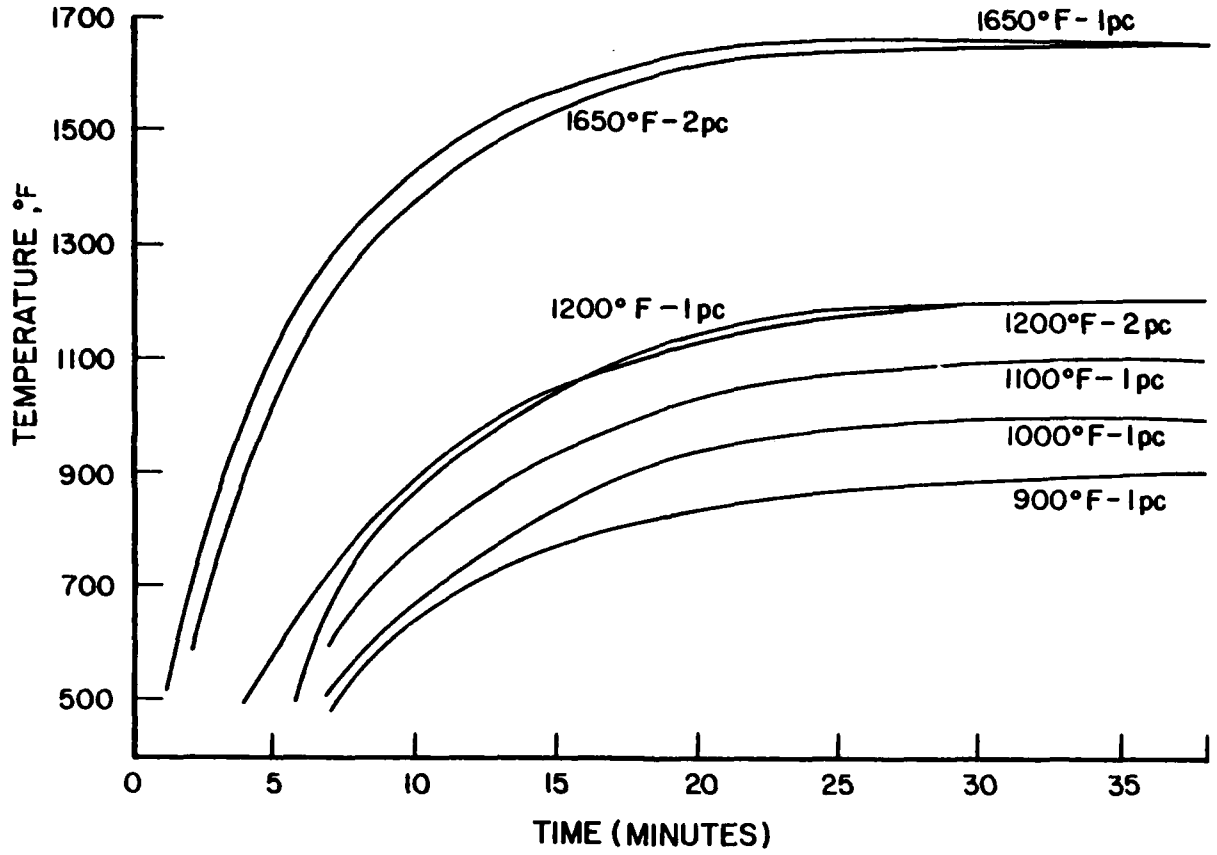

Figure 7. Heating rate curves for coupon to be used in test program. Curves show the time to reach either the austenitization or aging temperature.

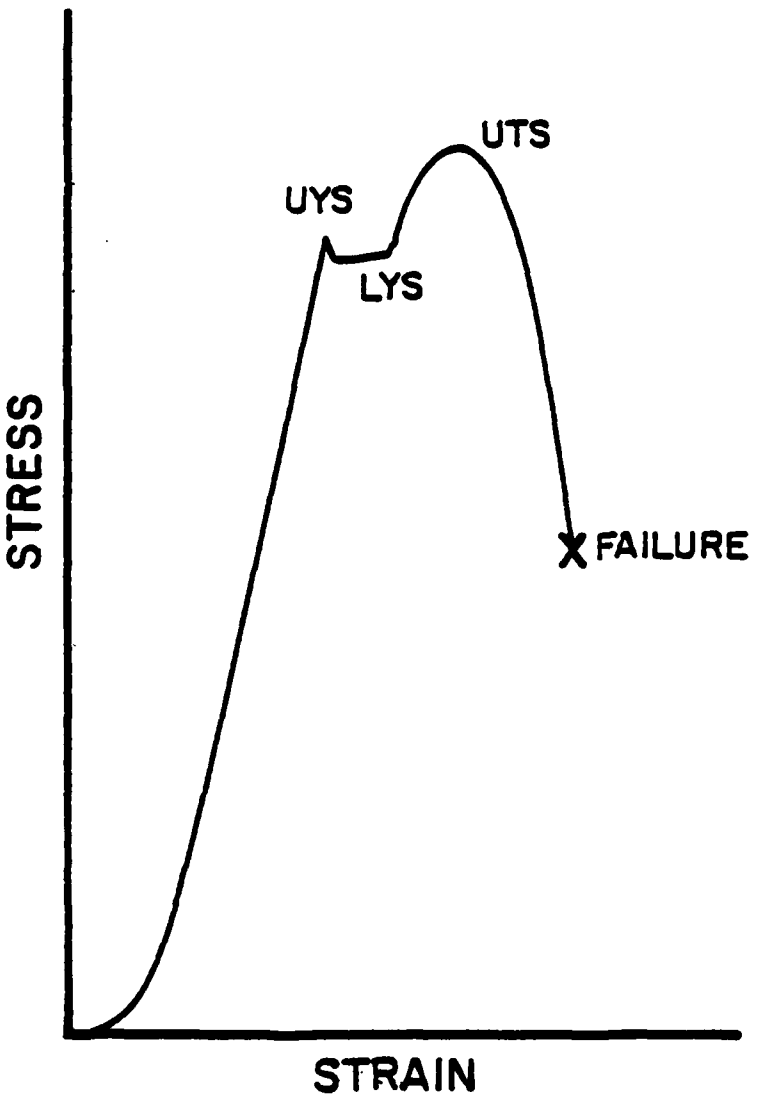

Figure 8. Typical stress/strain curve obtained for a tensile-test specimen.

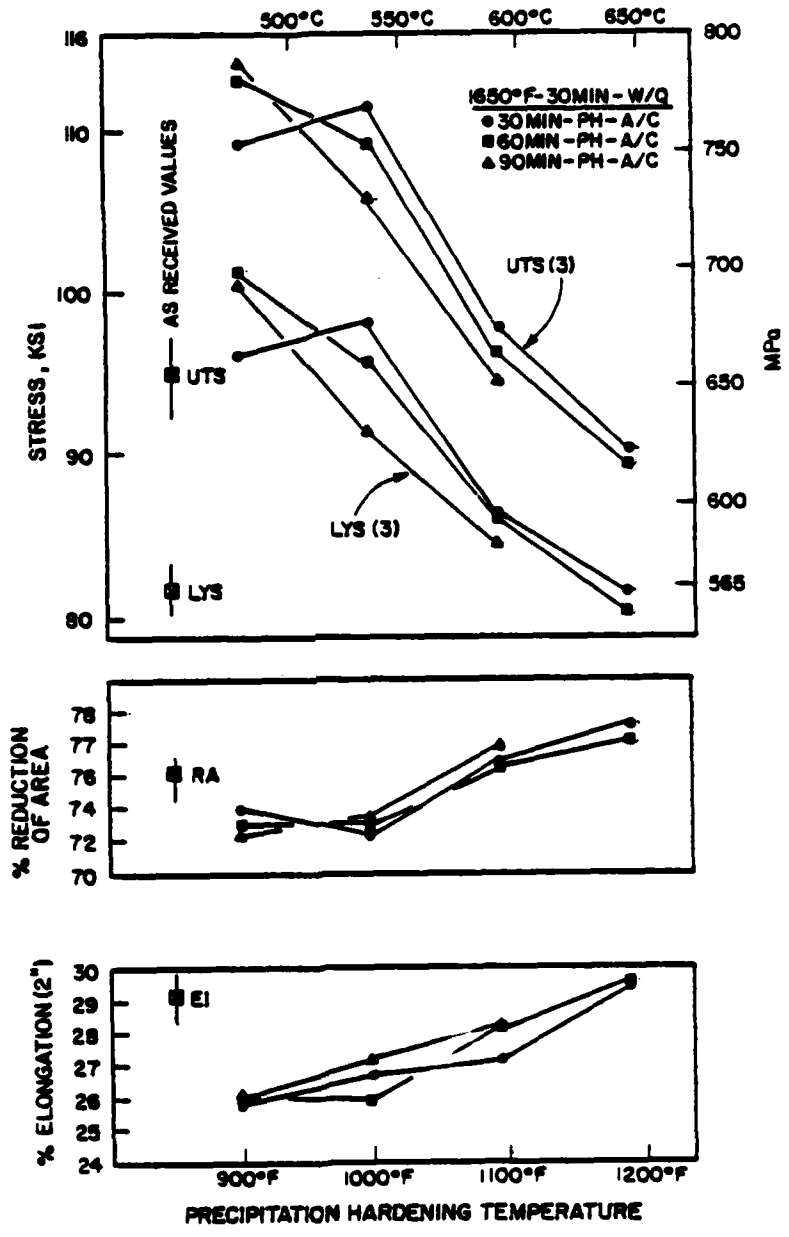

Figure 9. Tensile test results for specimens austenitized at 1650°F for 30 minutes and then aged at the indicated temperature.

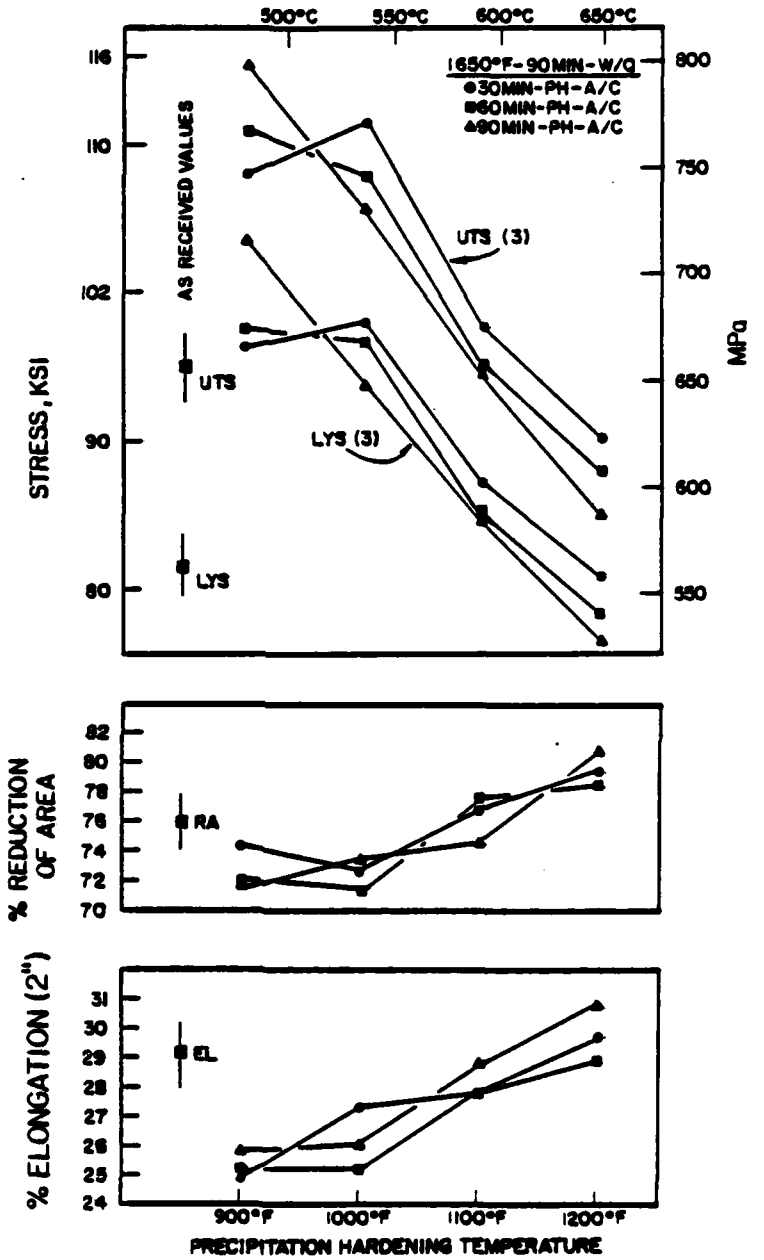

Figure 10. Tensile test results for specimens austenitized at 1650°F for 90 minutes and then aged at the indicated temperature.

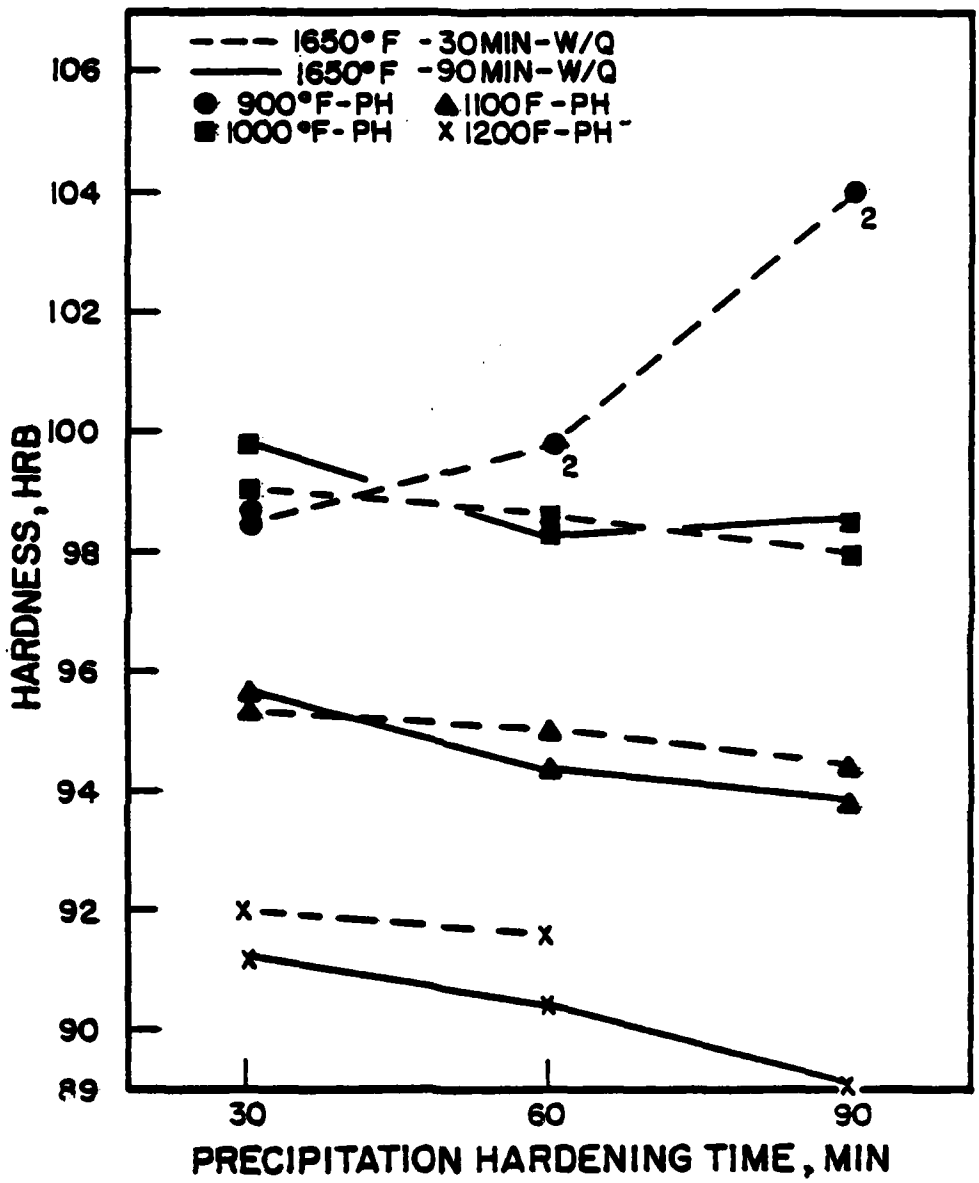

Figure 11. Hardness, HRB, versus precipitation hardening time in minutes.

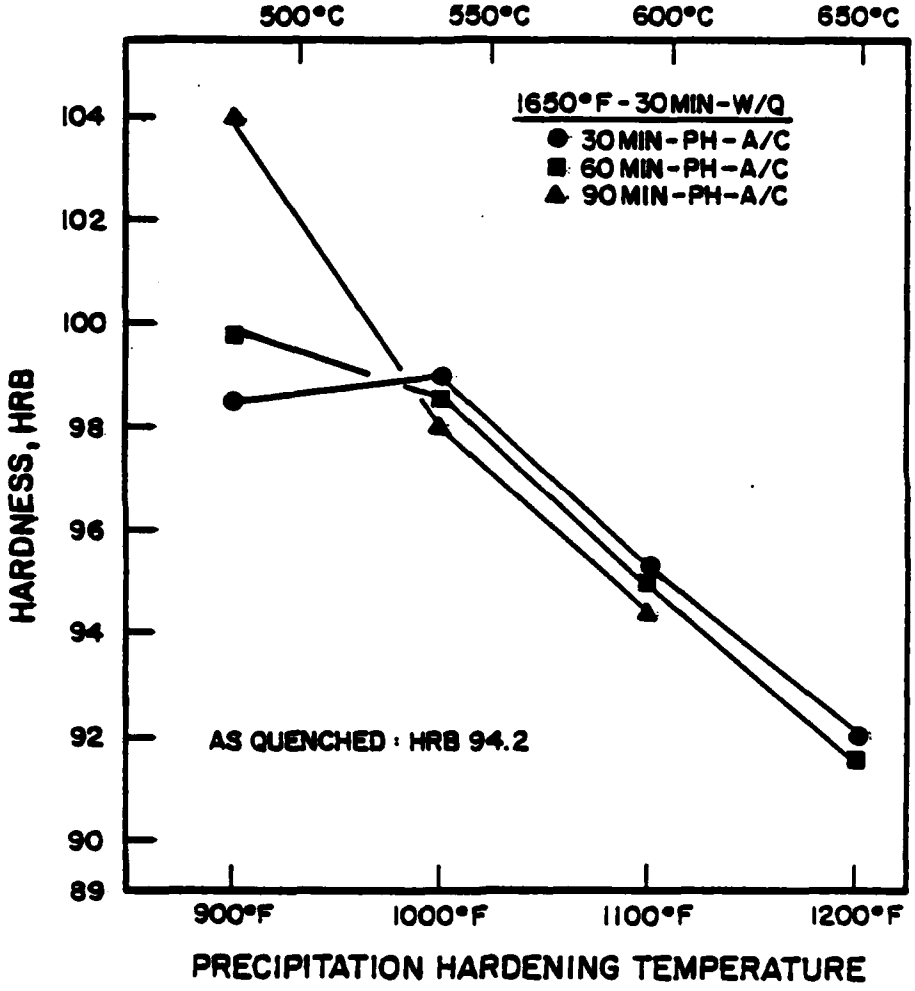

Figure 12. Hardness, HRB, versus precipitation hardening temperature for A710 austenitized at 1650°F for 30 minutes and then aged at the indicated temperature and time.

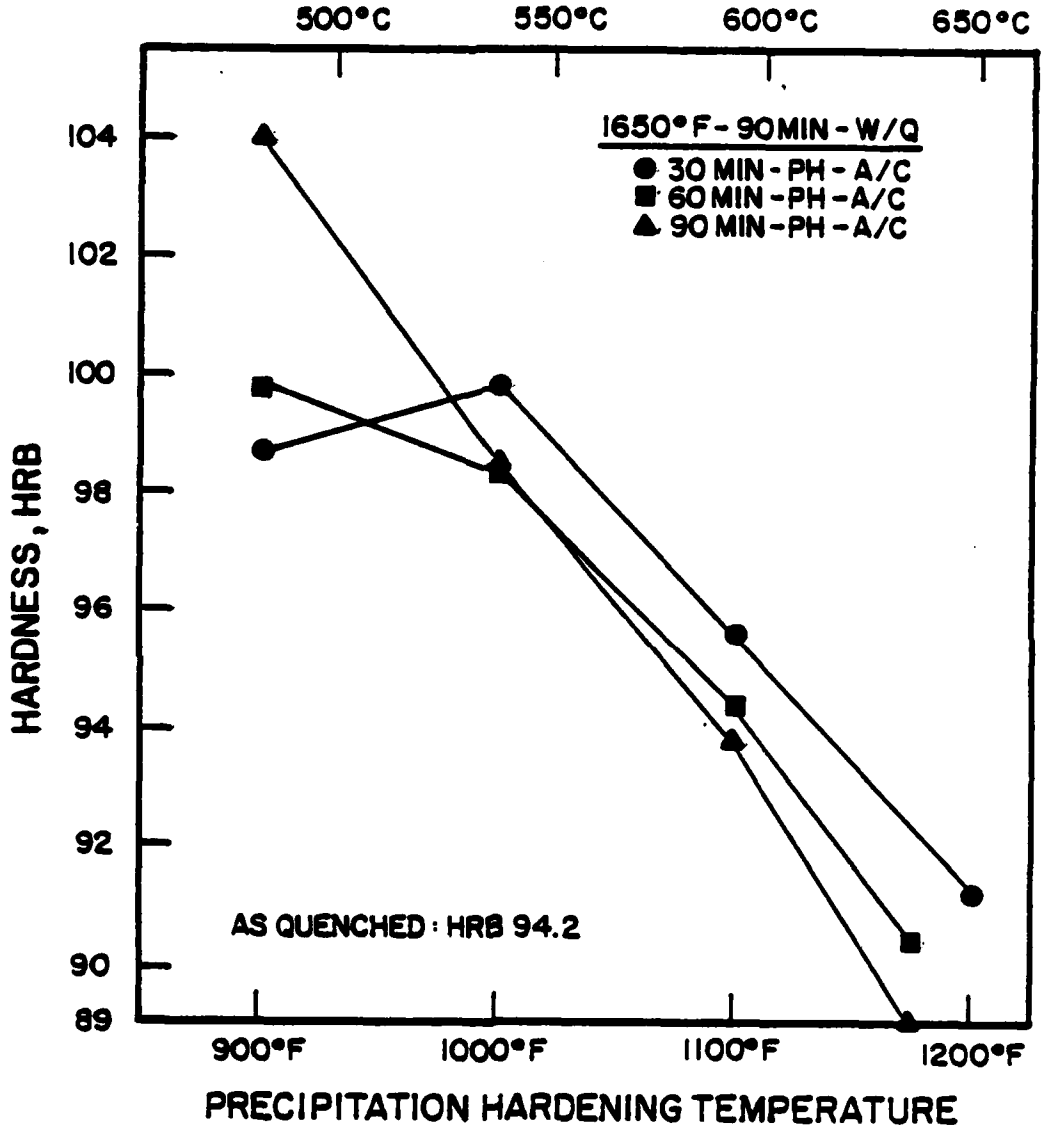

Figure 13. Hardness, HRB, versus precipitation hardening temperature for A710 austenitized at 1650°F for 90 minutes and then aged at the indicated tmeperature and time.

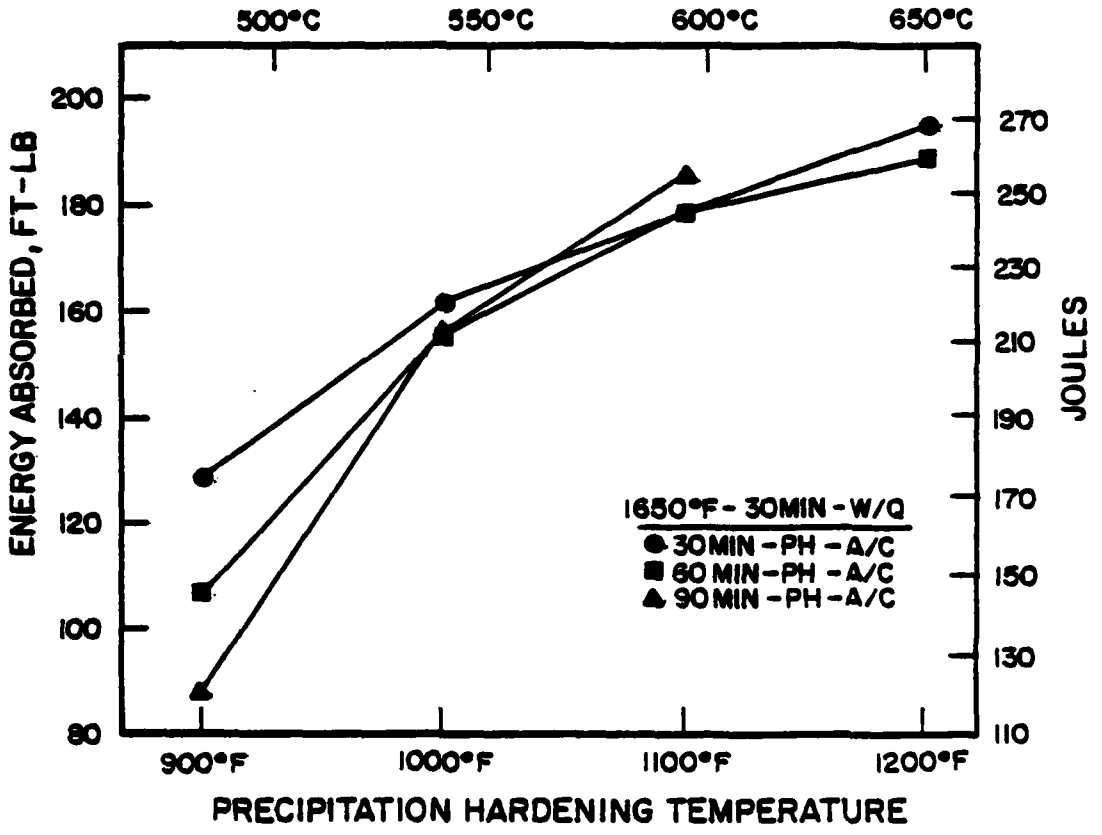

Figure 14. Energy absorbed versus precipitation hardening temperature for A710 austenitized at 1650°F for 30 minutes and then aged at the indicated temperature and time.

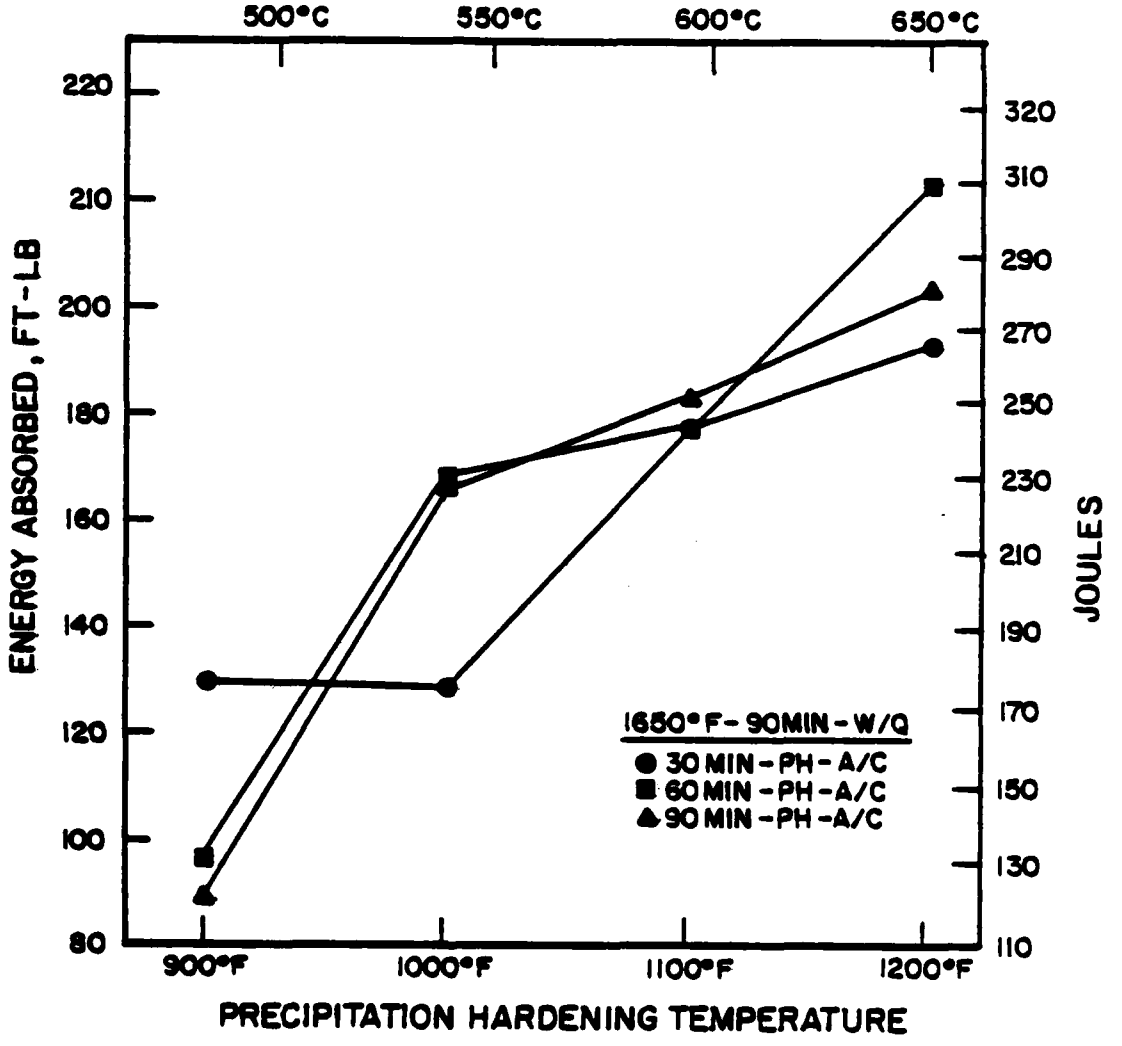

Figure 15. Energy absorbed versus precipitation hardening temperature for A710 austenitized at 1650°F for 90 minutes and then aged at the indicated temperature and time.

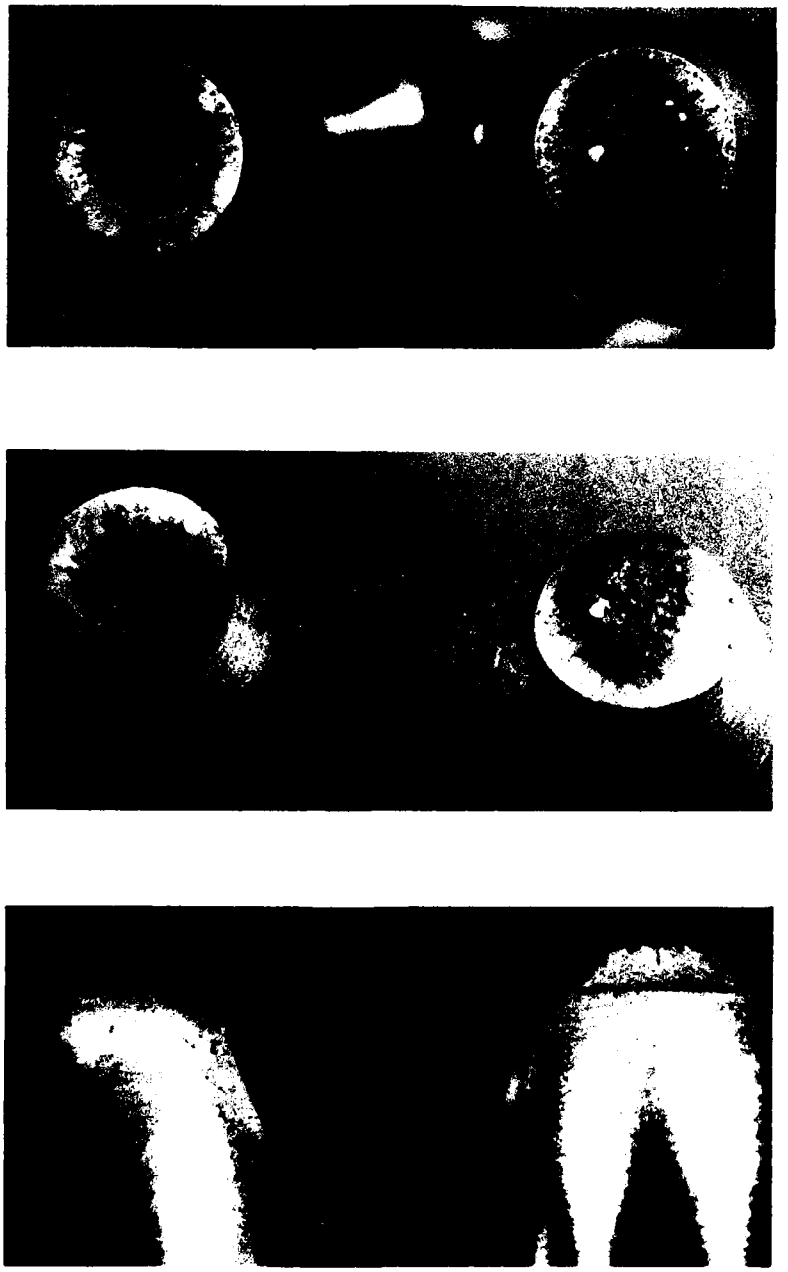

Figure 16. Fractured tensile specimens showing normal cup and cone fracture. X4

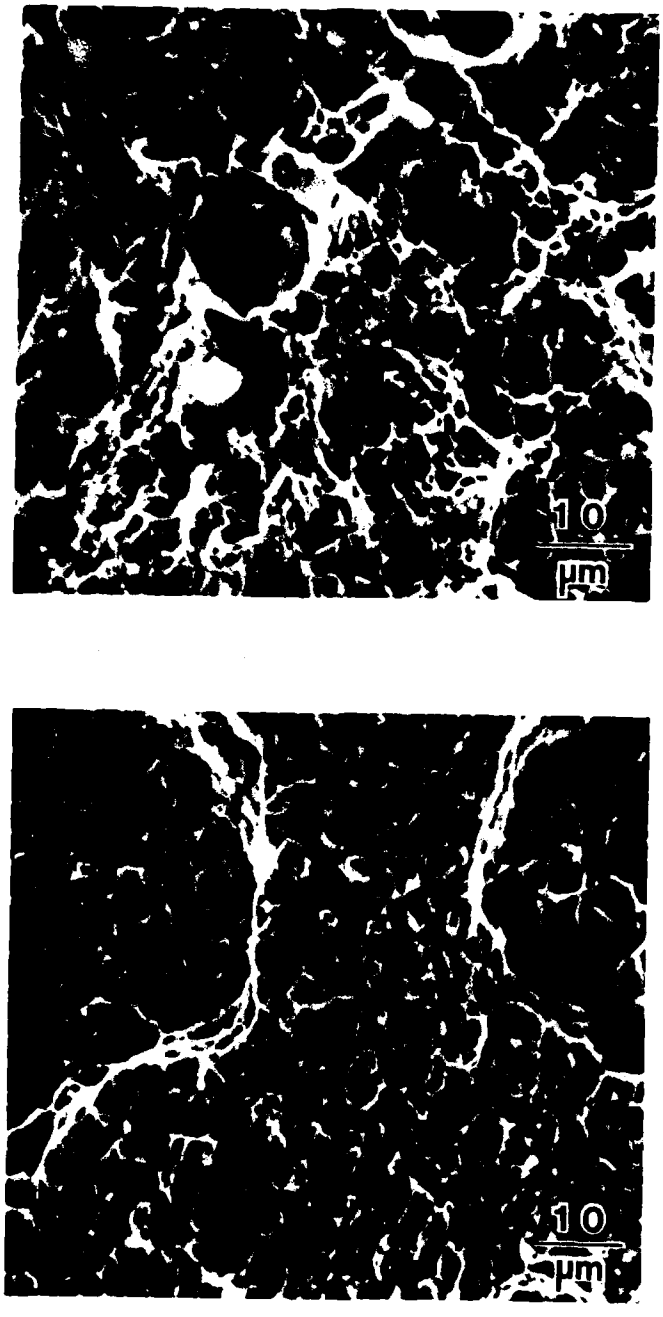

Figure 17. SEM observations of the cup and cone fractures. Failure mode is generally recognized as void-coalescence, more commonly as ductile fracture.

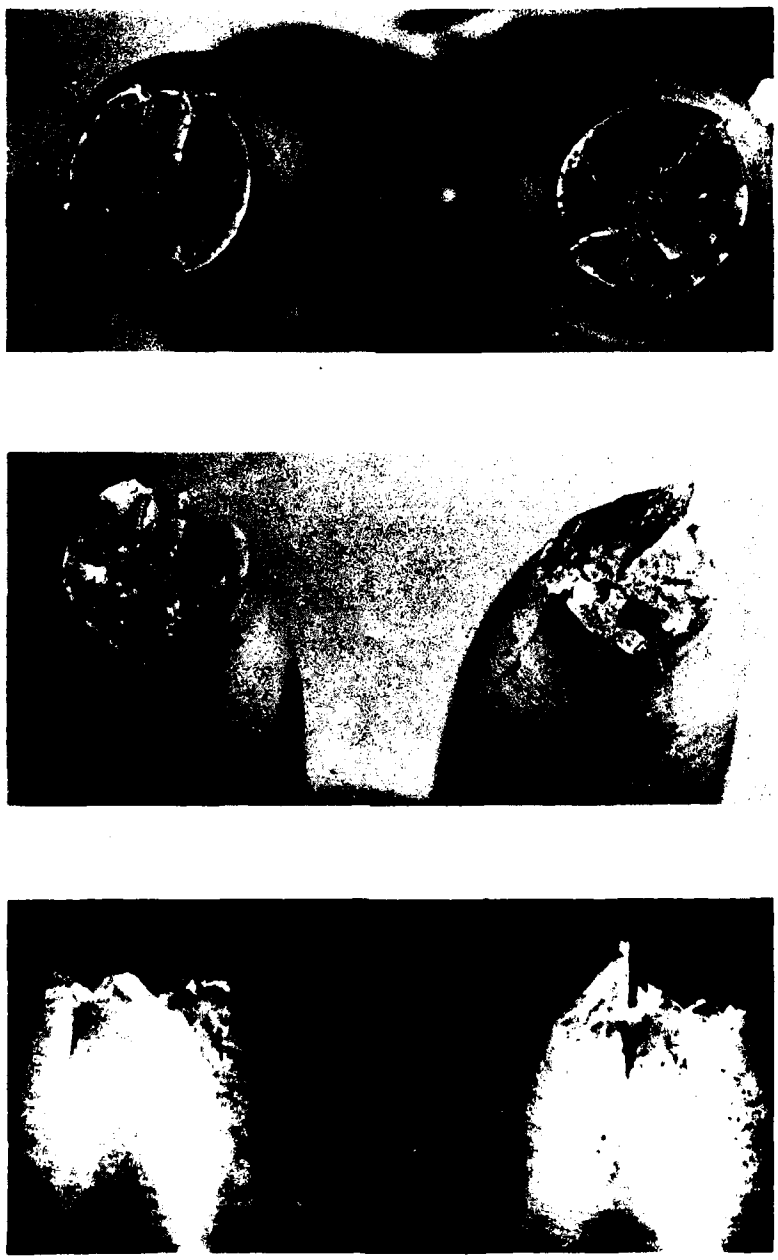

Figure 18. Macrographs showing the splitting observed in some broken tensile specimens. X4

Figure 19. SEM observations taken near the root of the splitting.

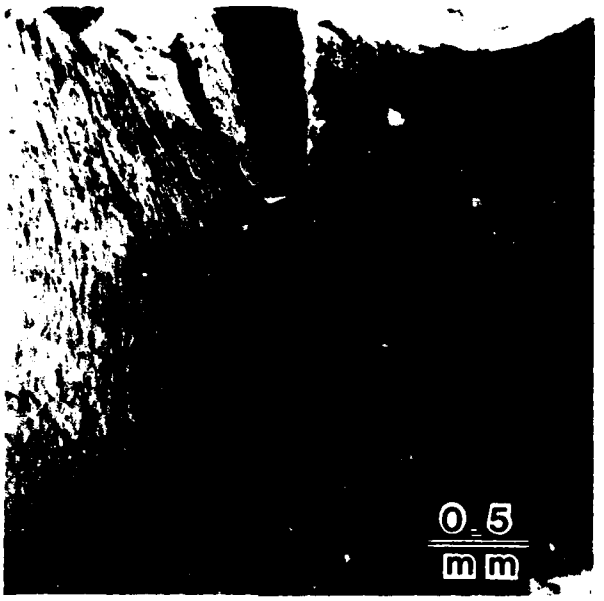

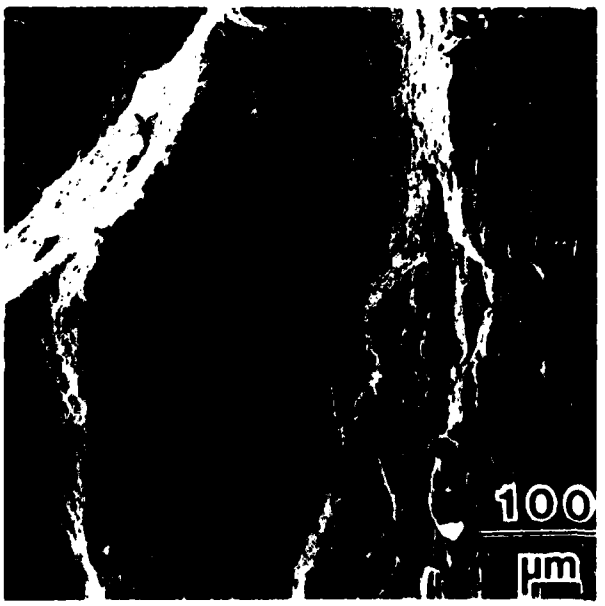

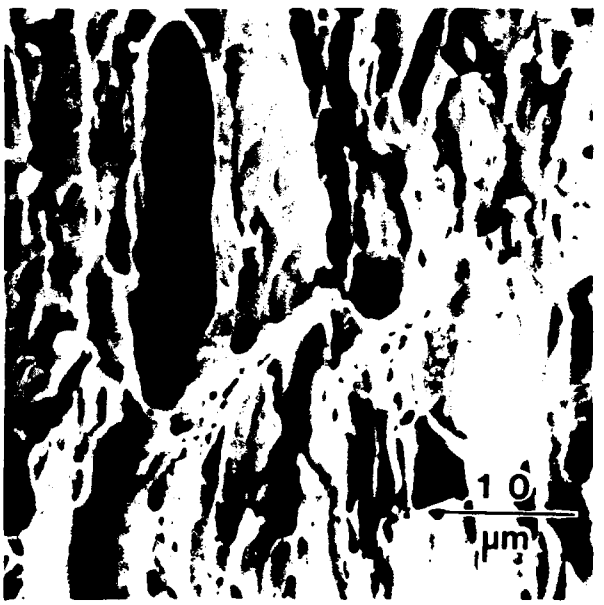

Figure 20. SEM observations within the split regions. All observations indicate fracture was ductile in nature.

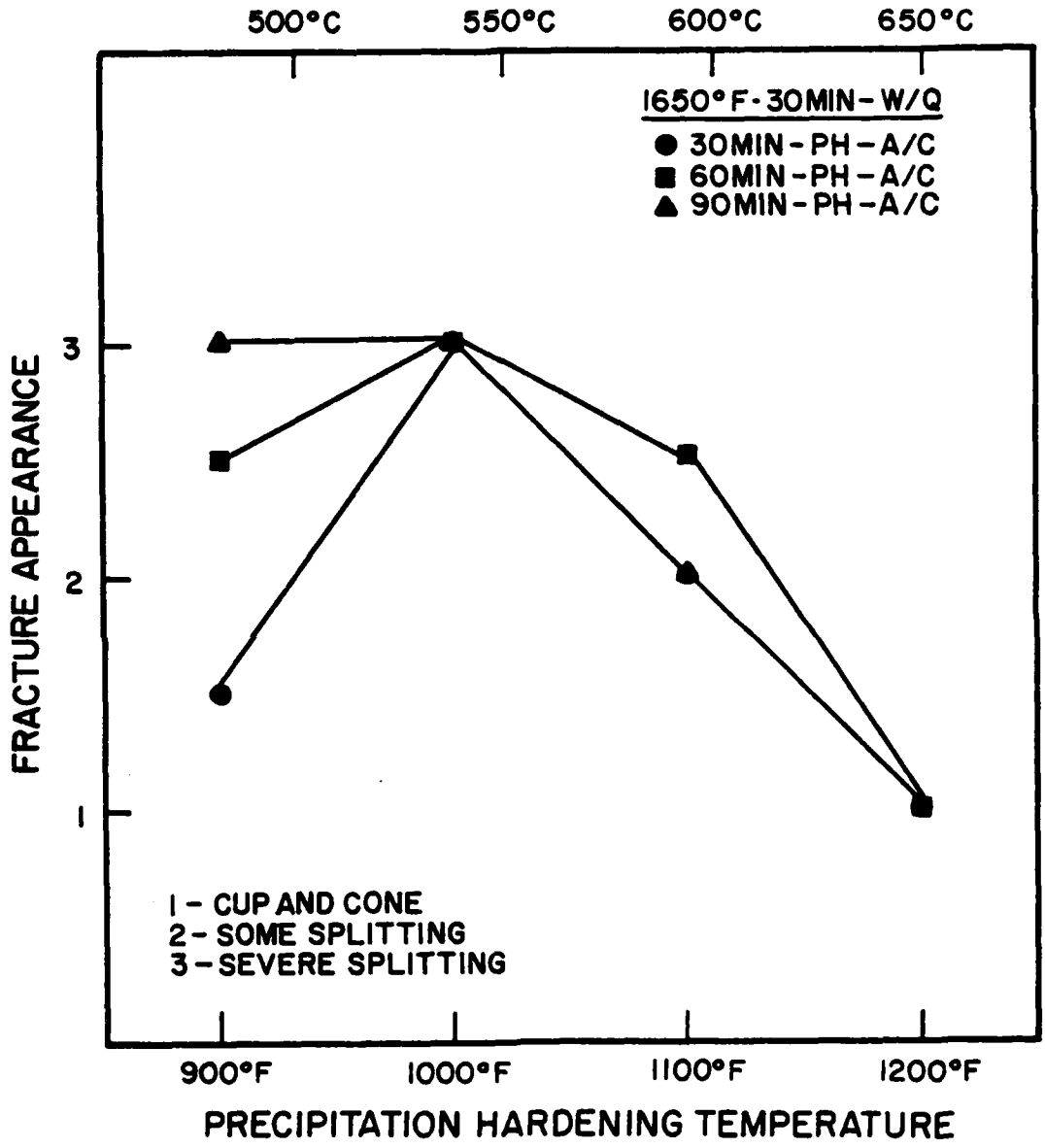

Figure 21. Fracture appearance versus precipitation hardening temperature for A710 austenitized at 1650°F for 30 minutes and then aged at the indicated temperature and time. The fracture appearance was that observed on broken .500 inch diameter tensile specimens.

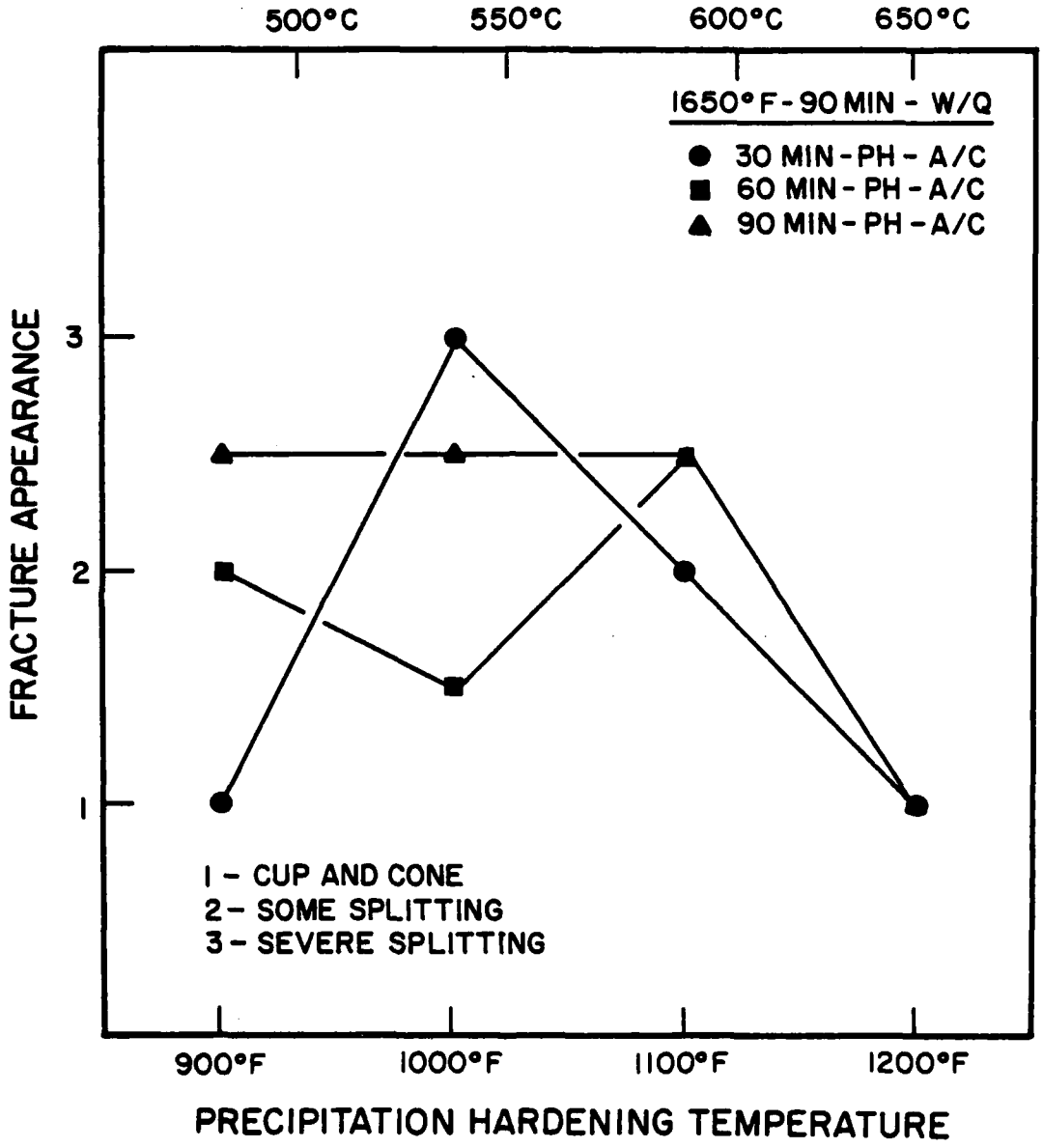

Figure 22. Fracture appearance versus precipitation hardening temperature for A710 austenitized at 1650°F for 90 minutes and then aged at the indicated temperature and time. The fracture appearance was that observed on broken tensile specimens.

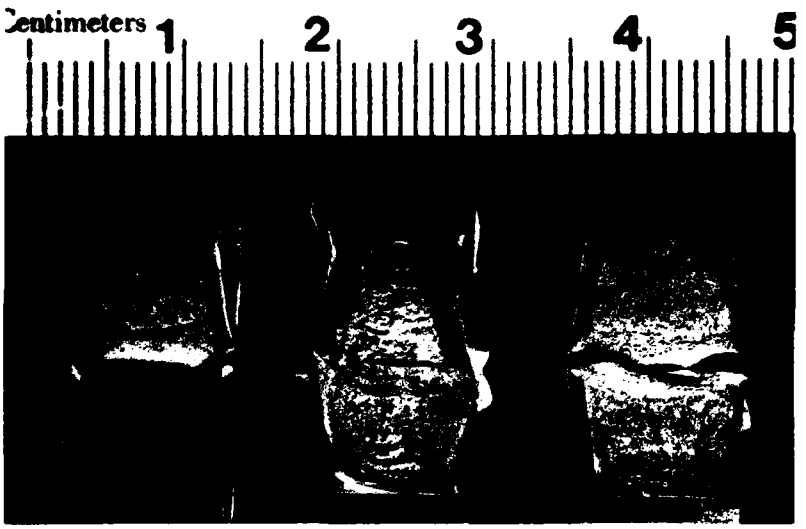

	1	29	21
Austenization Time, min.	30	As	90
Aging Temp., °F	900	Rec'd	900
Aging time, min.	30		90

Figure 23. Low magnification observations of broken impact specimens. These specimens, 1 and 21, were heat treated in an identical manner to those tensile specimens which showed splitting. Note the abscence of splitting in these specimens.

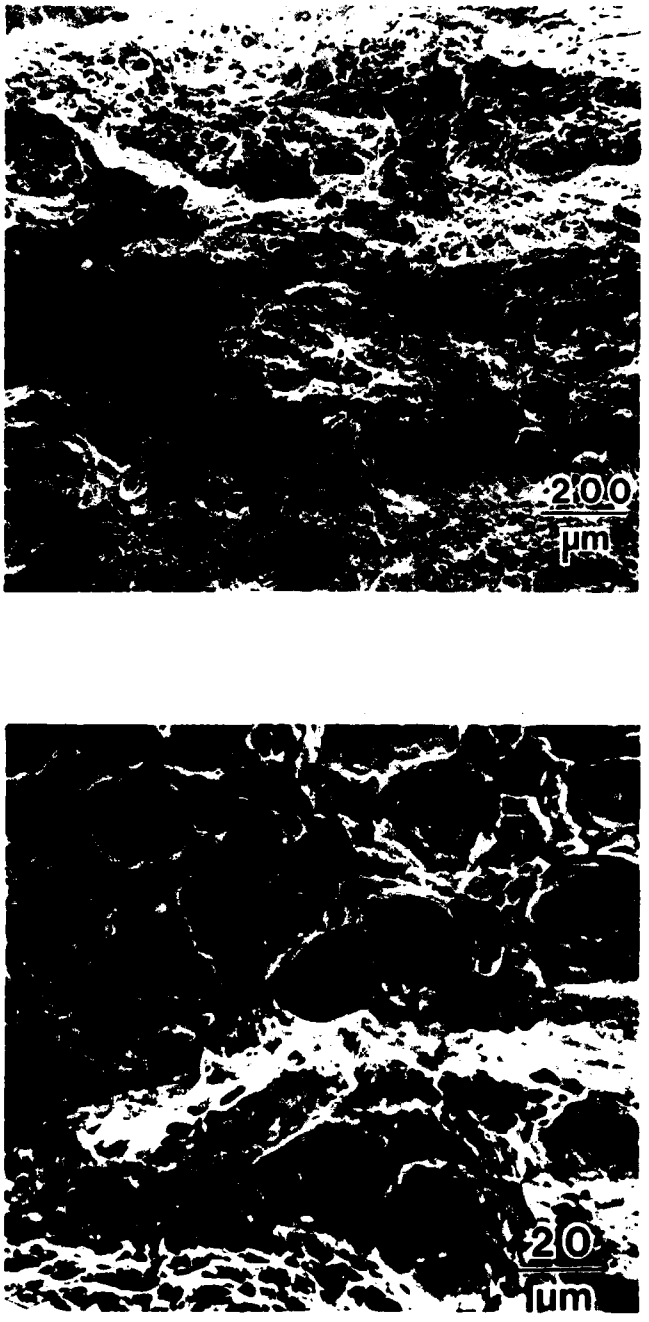

Figure 24. SEM observations of the impacts shown in Figure 23. Appearance is indicative of ductile fracture.

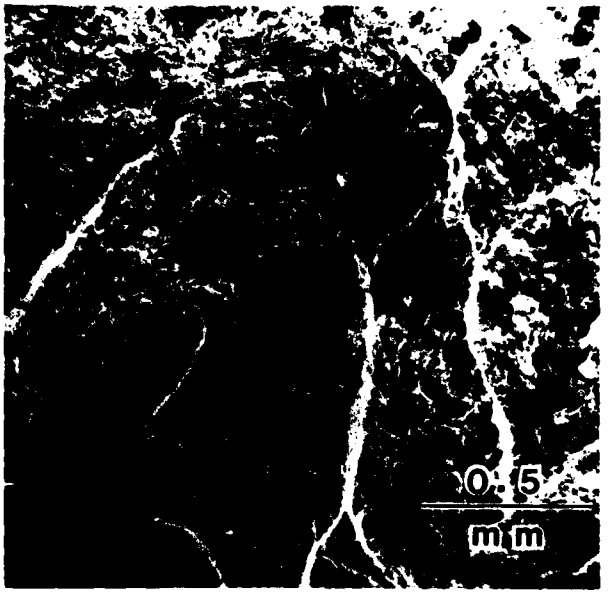

a

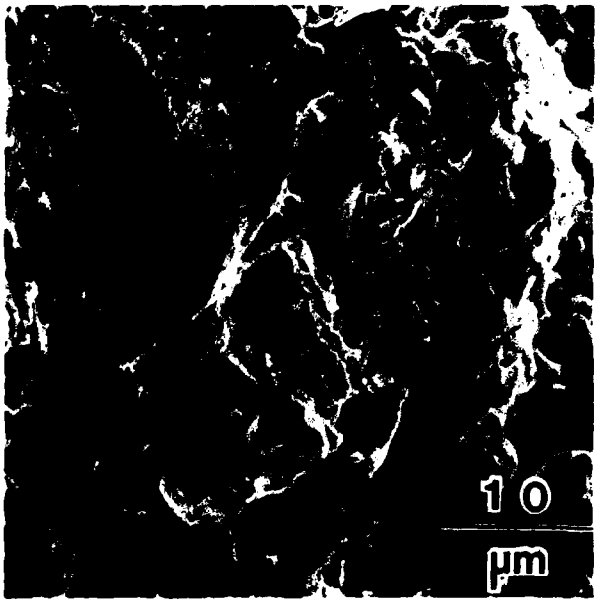

b

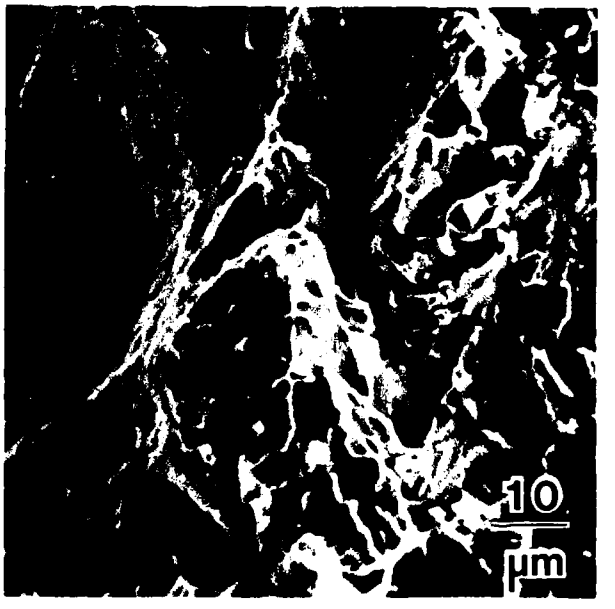

c

Figure 25. SEM observations of an impact specimen aged at 900°F and tested at 0°F. Surface (a), observed at higher magnifications (b) and (c), reveals cleavage fracture.

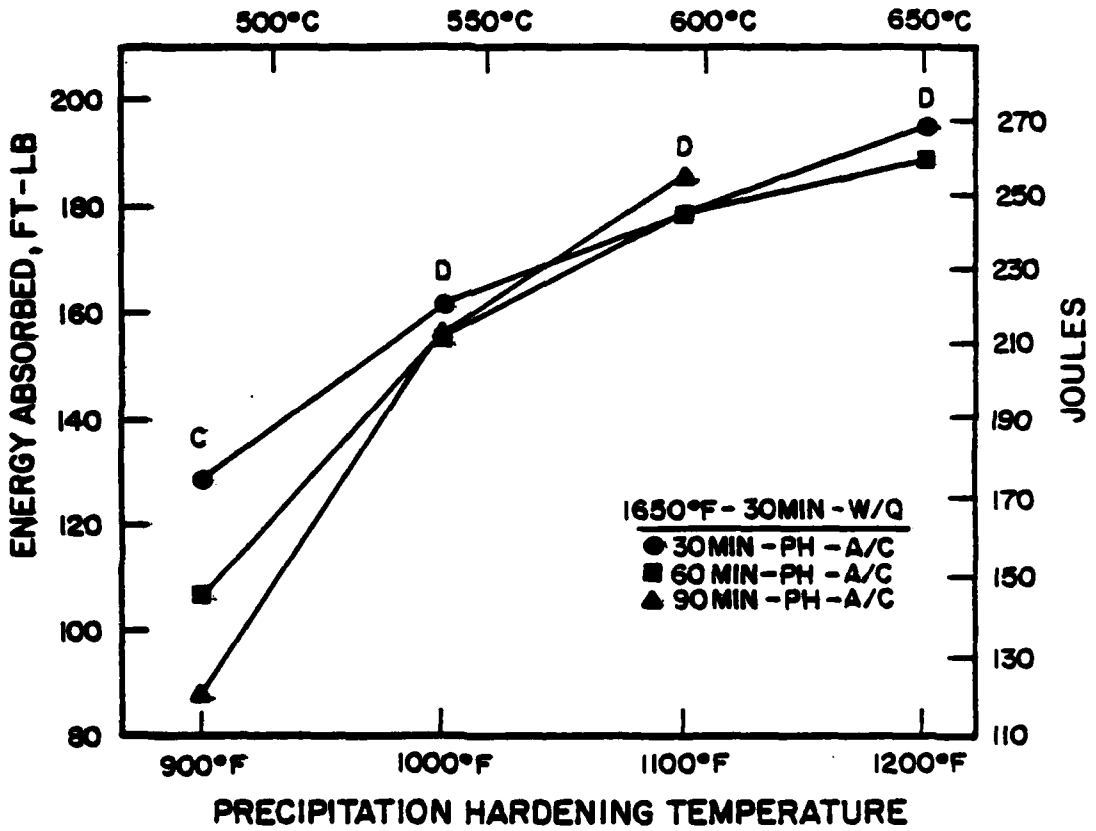

Figure 26. Energy absorbed versus precipitation hardening temperature for A710 austenitized at 1650°F for 30 minutes. Letters C and D refer to the type of fracture exhibited on the broken impact specimens. C is cleavage, and D,ductile fracture.

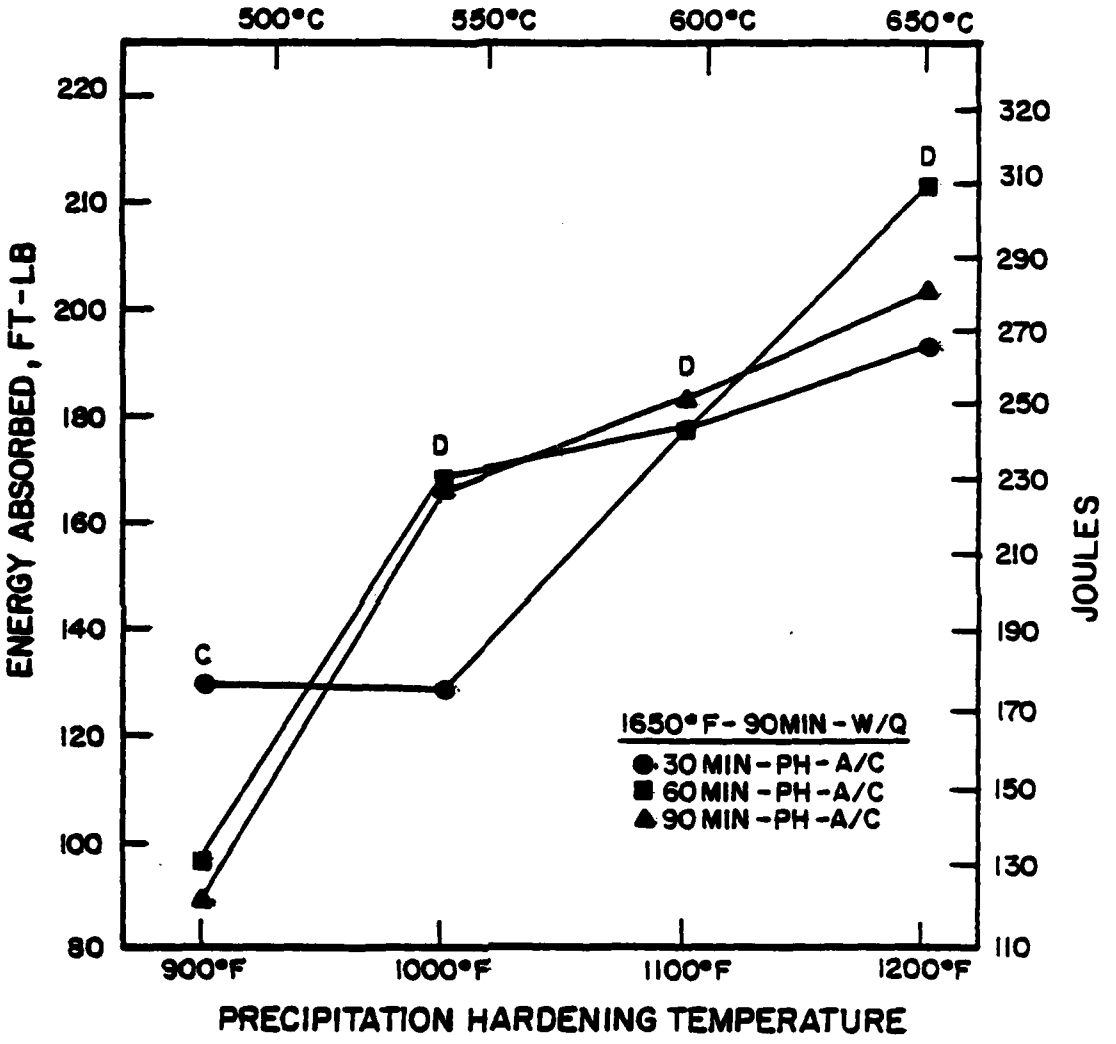

Figure 27. Energy absorbed versus precipitation hardening temperature for A710 austenitized at 1650°F for 90 minutes. Letters C and D refer to the type of fracture exhibited on the broken impact specimens. C is cleavage and D,ductile fracture.

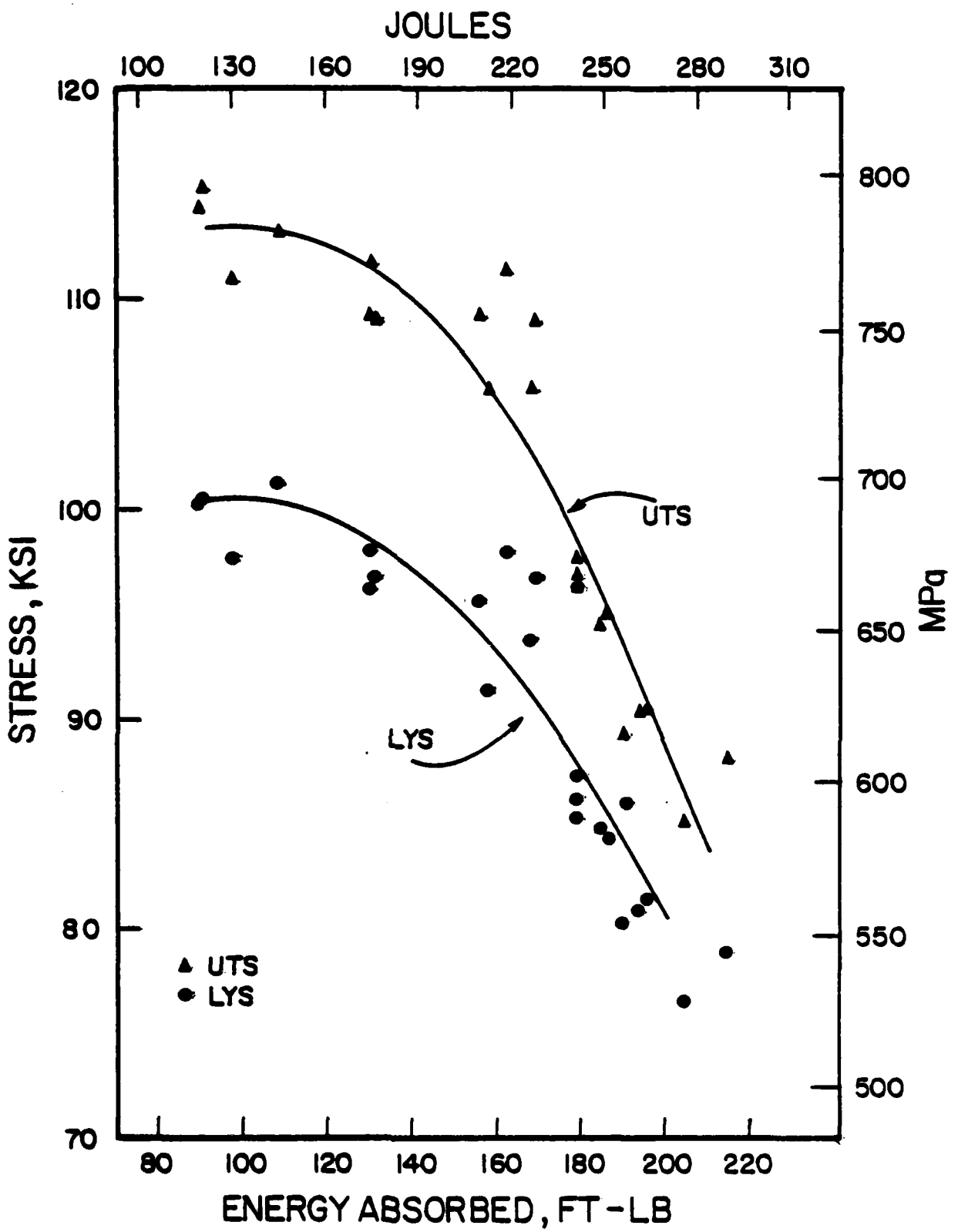

Figure 28. Ultimate tensile stress and lower yield stress versus energy absorbed.

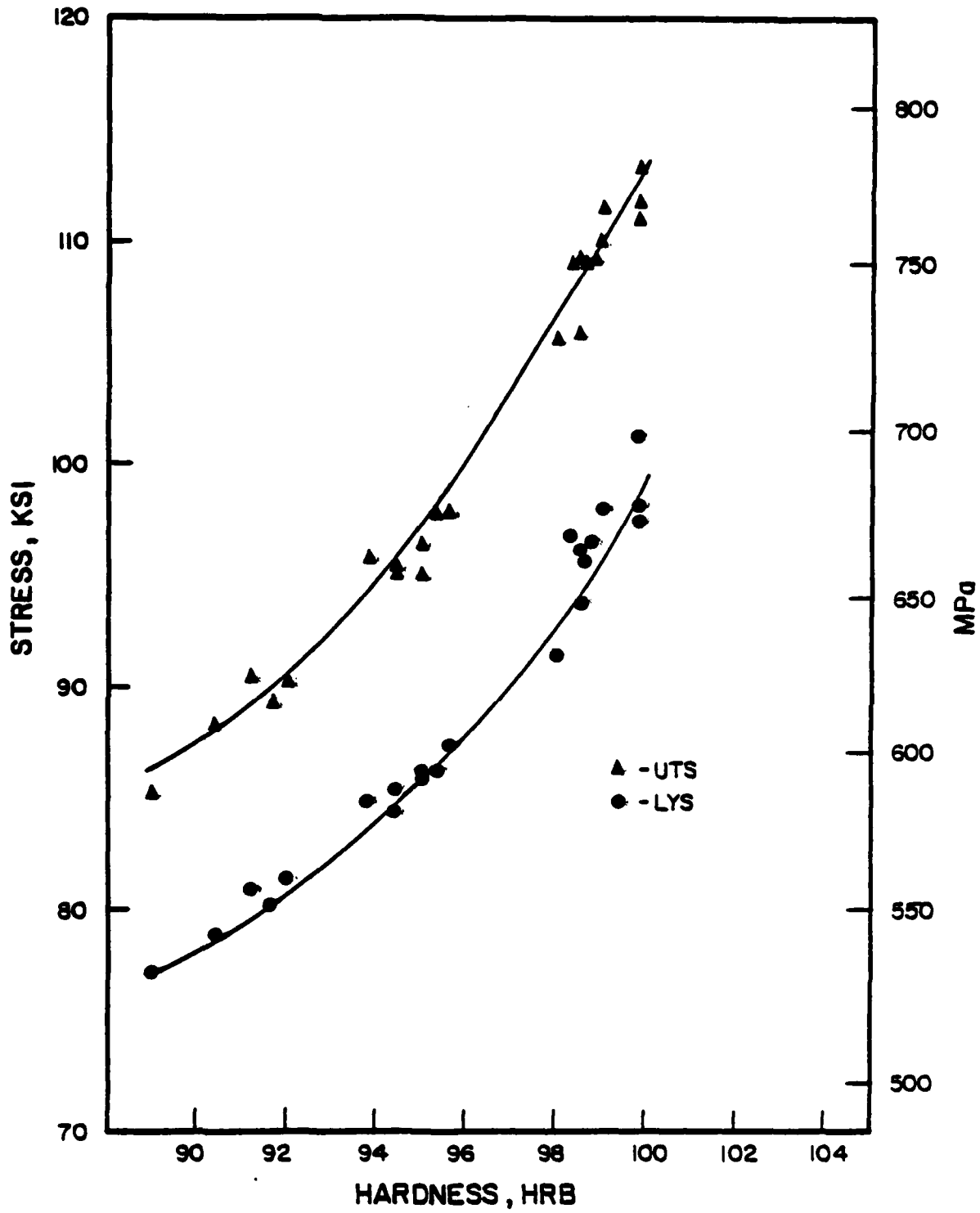

Figure 29. Ultimate tensile stress and lower yield stress versus hardness, HRB.

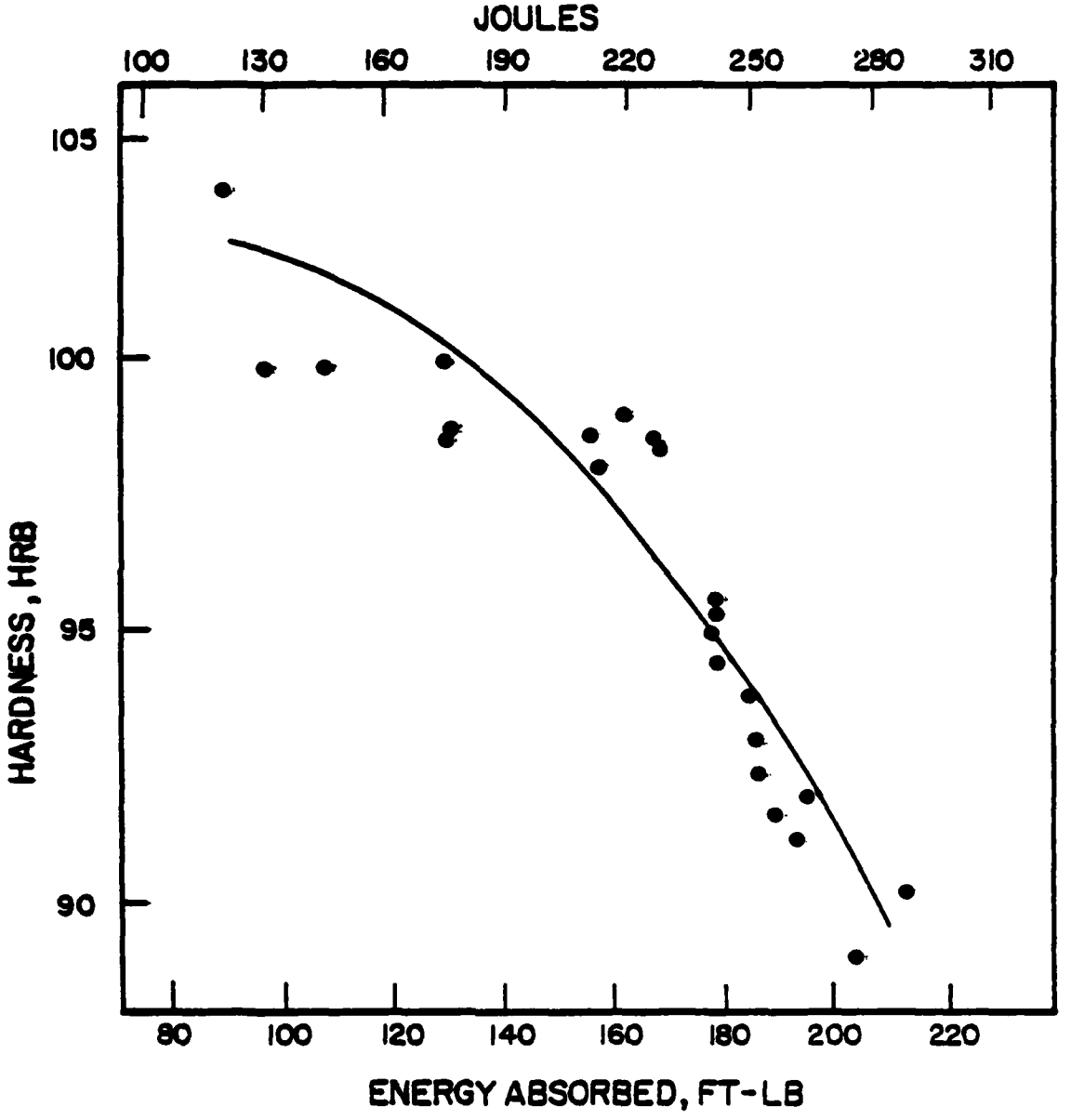

Figure 30. Hardness, HRB, versus energy absorbed for each test condition.

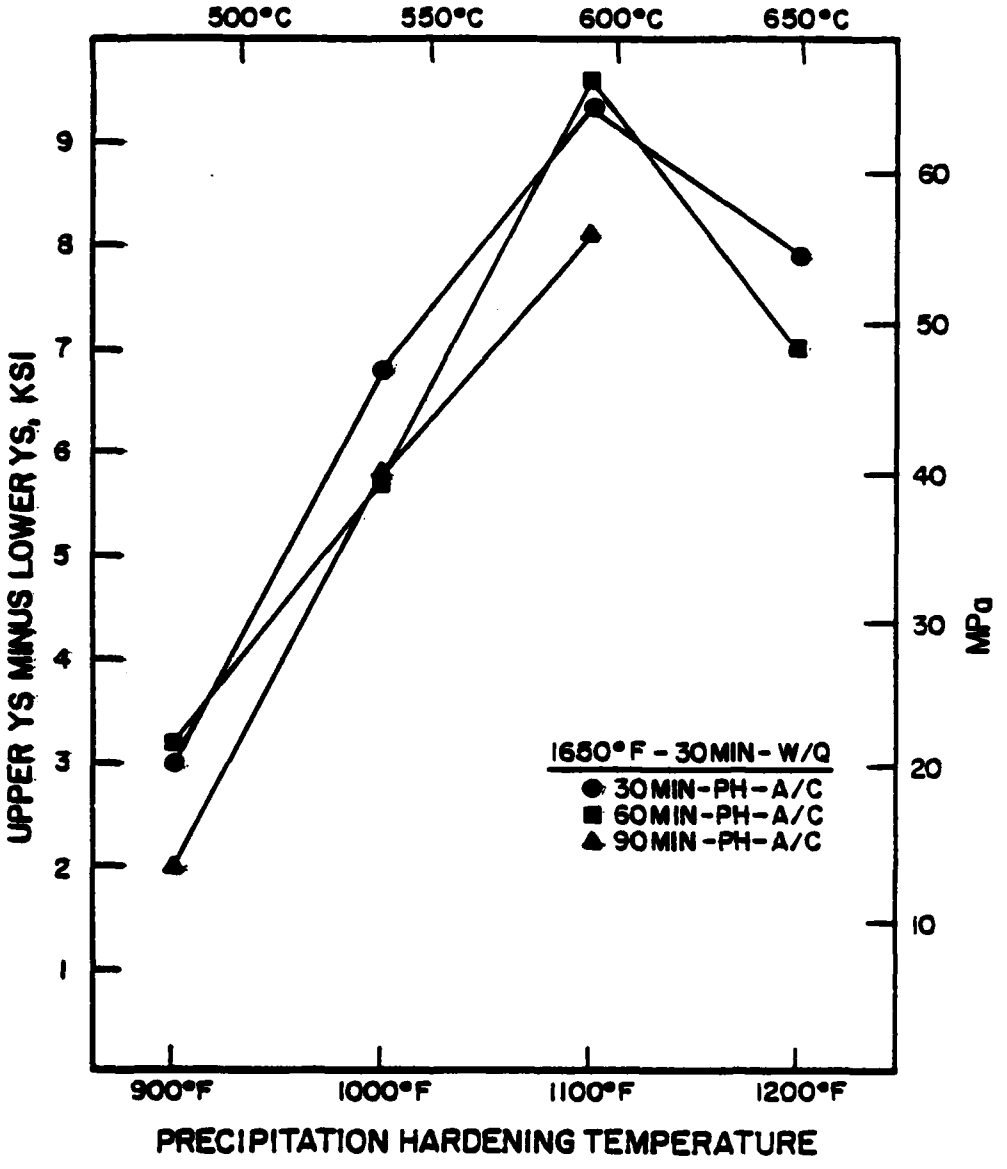

Figure 31. Upper yield stress minus lower yield stress versus precipitation hardening temperature for A710 austenitized at 1650°F for 30 minutes and then aged at the indicated temperature and time.

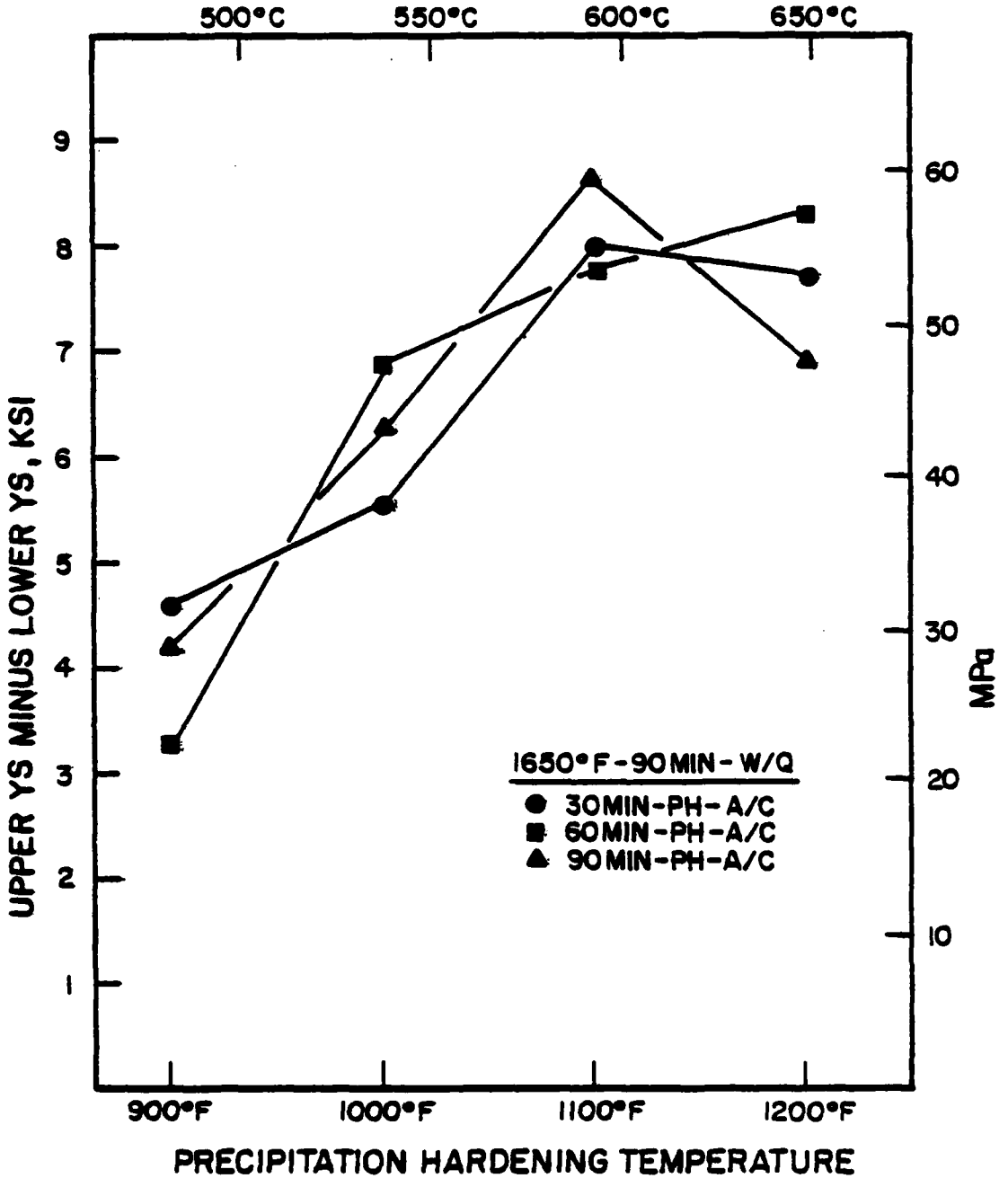

Figure 32. Upper yield stress minus lower yield stress versus precipitation hardening temperature for A710 austenitized at 1650°F for 90 minutes and then aged at the indicated temperature and time.

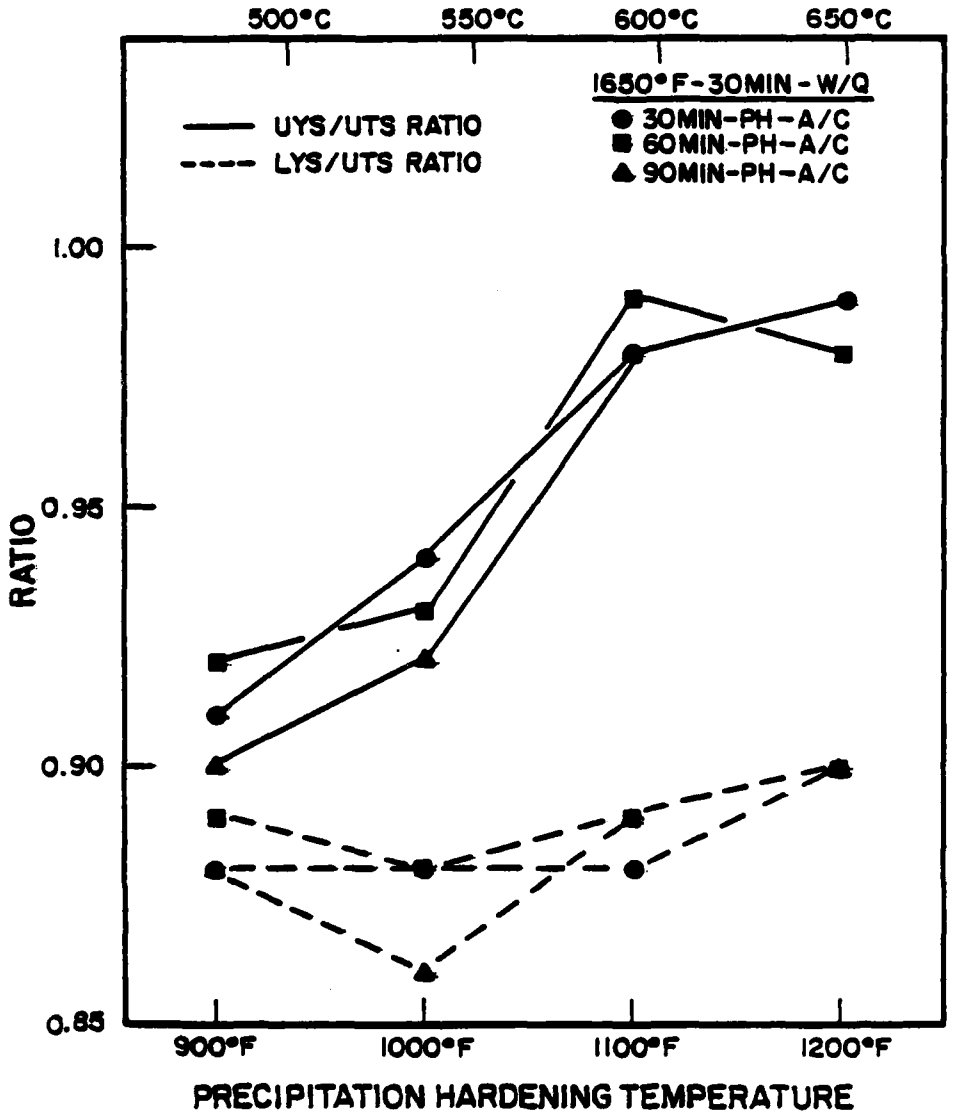

Figure 33. Ratio of upper yield stress, lower yield stress to the ultimate tensile stress versus precipitation hardening temperature for A710 austenitized at 1650°F for 30 minutes and then aged at the indicated temperature and time.

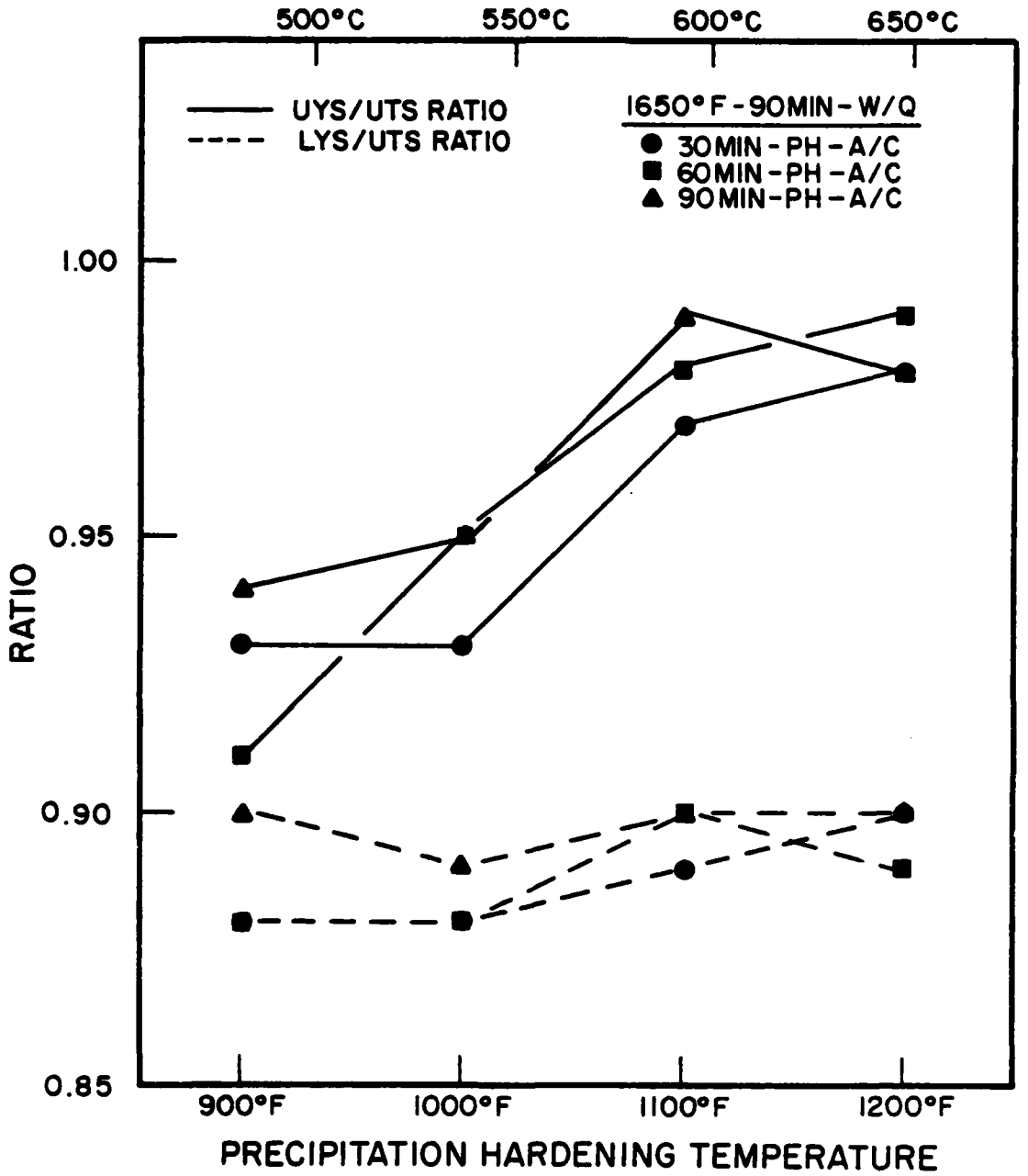

Figure 34. Ratio of upper yield stress, lower yield stress to the ultimate tensile stress versus precipitation hardening temperature for A710 austenitized at 1650°F for 90 minutes and then aged at the indicated temperature and time.

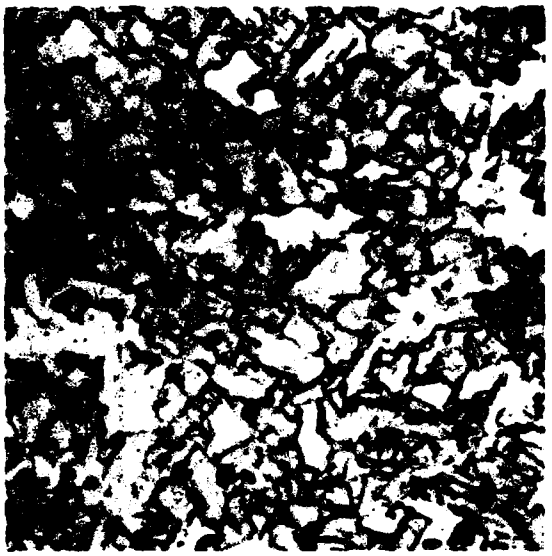

a
1650°F-30 min - W/Q
900°F-30 min - A/C

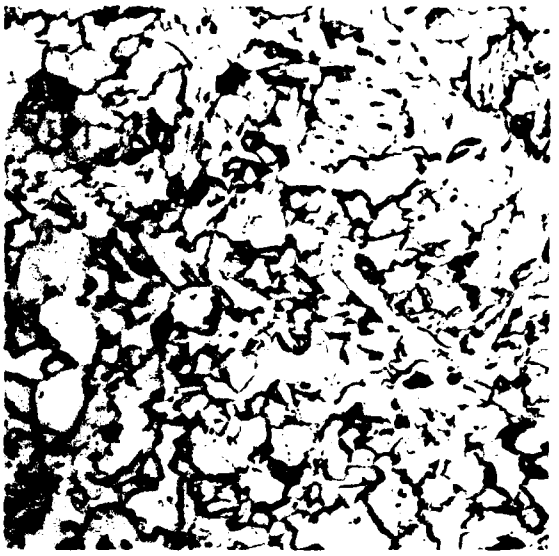

b
1650°F-90 min - W/Q
900°F-30 min - A/C

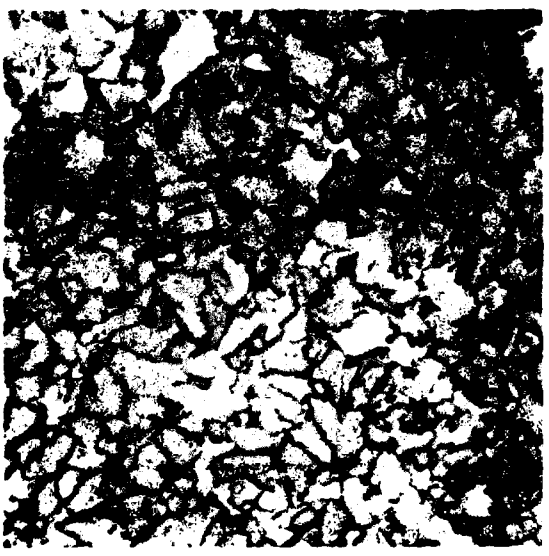

c
1650°F-30 min - W/Q
1200°F-90 min - A/C

d
1650°F-30 min - W/Q
1200°F-90 min - A/C

Figure 35. Representative microstructures for the various austenitizing, aging, temperatures and times. Photographs clearly show that is almost impossible to distinguish between the heat treatments. All X1000

Acknowledgment

The authors thank L.K. Ives for his efforts in the electron microscopy investigation. And we are pleased to acknowledge our secretaries, Ms. D. Easterday and Mrs. P. Salpino, both of whom worked so diligently on the manuscript.

APPENDIX A.

TITLE: Small Angle Neutron Scattering (SANS) Study of Aging of ASTM A710 Grade A, Class 3 Steel

SUBMITTED TO: Dr. Richard Fields and George Hicho
Fracture and Deformation Division
National Bureau of Standards
Gaithersburg, MD

BY: Dr. Satish P. Singhal

INTRODUCTION

Recently, a low carbon precipitation hardenable alloy steel, A710, has been considered for high strength, welded structures. Strengthening of A710 takes place by controlled precipitation of copper rich particles in a ferrite matrix at temperatures below 1300°F. The goal of this small-angle neutron scattering (SANS) study was to find a correlation between aging treatment (duration and temperature), mechanical properties (hardness), and SANS characteristics.

SAMPLES AND EXPERIMENTAL PARAMETERS

Prior to aging all samples (0.11m thick) were austenitized at 1650°F for about 90 minutes. Solution treatment was terminated by water quenching. Aging was carried out in the temperature range of 900 to 1200°F for times 30 min to 90 min. Other sample details are given in Table 1. SANS investigations were carried out in the scattering vector (Q) range 0.001 to 0.013 nm^{-1}. In this Q range the contribution of the precipitates in the size range of 4.8 to 60nm is measured.

The detailed theory for data reduction has been discussed by Kostorz (2). A few salient features, however, are described here. Let us assume that Ip is the intensity scattered by the sample containing the precipitates, then following Kostorz (2):

$$I_p(Q) = M_p\ \phi_o\ t_p\ T_p\ \Delta\Omega\ \varepsilon_d \quad \frac{d\Sigma^p_{SCatt}}{d\Omega} \qquad (1)$$

where

M_p = total monitor count,

ϕ_o = neutron flux on the sample - per monitor count,

t_p = sample thickness,

T_p = sample transmission

ε_d = detector efficiency

Δ_Ω = solid angle of one detector element at the scattering vector Q,

$\frac{d\Sigma^p_{Scatt}}{d\Omega}$ = macroscopic differential scattering cross-section of the sample

Differential scattering cross-section is the "bulk averaged" measure of the precipitate volume fraction, precipitate size distribution, and "scattering contrast" between the matrix and precipitates. Scattering contrast in this case depends upon the difference in the Cu content in the matrix and the precipitates. Additional contrast comes into the play due to the magnetic nature of the ferrite matrix as precipitates themselves are non-magnetic.

It is clear from equation 1 that as long as we divide all the sample's intensity (Ip(Q)) by the thickness (t_p) and transmission (T_p) we can intercompare the spectra from various samples after adjusting the counts to the same monitor value (M_p). ϕ_o and εd are the instrumental constants and do not change, whereas the program "AVERAGE" normalizes for the variation of $\Delta\Omega$ with Q, as well as calculates the intensities at each scattering vector. Further details of data processing will be described in the results and discussion section. Other SANS experimental parameters are given in Table (2).

CONSIDERATIONS RELATING SANS WITH PRECIPITATION PHENOMENA.

The central idea in understanding the precipitation phenomena in supersaturated solid-solutions is that first nucleation takes place and then these nuclei grow by diffusion controlled mechanisms. For an alloy of fixed composition the aging temperature dictates the number of particles (nuclei) cm^{-3} in the specimen and aging time determines their size distribution. At longer aging times, the number of particles cm^{-3} (N_v) reduces because large particles grow at the expense of smaller ones by a mechanism called "Ostwald ripening". Following Guinier (2) for a system of "randomly" distributed particles the macroscopic cross-section ($d\varepsilon/d\Omega$) (see eq. 1) can be given as:

$$\frac{d\Sigma}{d\Omega} = (\zeta_p - \zeta_m)^2 \cdot V_p^2 N_p \cdot \exp\frac{(-Q^2 \cdot R^2)}{3} + \psi(Q) \qquad (2).$$

Here ζ_m, ζ_p = Scattering length density of the matrix (m) and precipitate (P).

V_p, N_p = Volume of one precipitate (V_p) and number of precipitates in the sample (N_p).

R = Radius of gyration related to the particle diameter as $D = 2R\sqrt{5/3}$.

$\psi(Q)$ = Interparticle interference function which is negligible in case of low volume fractions of precipitates in the matrix.

In cases where $\psi(Q)$ is significant a peak at $Q \neq 0$ is seen in the scattering curve.

The Guinier law, Eq 2, has some limitation in the sense that it considers the particulate assembly to be monodispersoid. One could, however, analyze low Q regions of the scattering curves in order to get useful information about the "average" size growth of the precipitates with thermal treatment. One can also see from Eq 2 that with an increase of R (or D), the slope of a

log $d\Sigma/dr$ vs Q^2 curve will increase, signifying the size growth of the precipitates. Where such growth takes place, the scattering curve translates to lower scattering vectors, i.e., intensity at low Q rises but at high Q, it goes down. This is schematically shown in figure 35. The temporal cross-over between two subsequent scattering curves (e.q. at Qc. in Figure 1) is the hallmark of such coarsening process.

RESULTS AND DISCUSSIONS

General Remarks

Since precipitation phenomena in A710 involves the nucleation and growth of a non-magnetic phase within the magnetic ferrite matrix, it is necessary to eliminate magnetic scattering from the matrix in order to measure only the nuclear (contrast) scattering between the precipitate and matrix. This was accomplished by applying a $\sim$ 6K Gauss magnetic field in the direction perpendicular to the neutron beam across the sample. The resultant 2-dimensional detector pattern for the sample #23 is shown in Figure 2. One can see that the resulting intensity in the field direction (H) decreases because all the moments are aligned along it. This results in a familiar "figure of eight" pattern seen very commonly for magnetic samples. In Figure 2, direction H, one sees only nuclear contrast scattering whereas in the direction perpendicular to H, one sees nuclear plus magnetic scattering. Similar patterns were seen for all other samples as well. In Figure 3 we show the scattering curves in the field direction and perpendicular to it. This averaging was done by cutting a 30° sector along the H and perpendicular to the H (Figure 2) and averaging both sides of the detector. One can see (Figure 3) that for a given Q the scattered intensity in the field direction is always lower than in the perpendicular direction.

Some interesting conclusions can be drawn from the Guinier plot in Figure 3. In a monodispersed system, where all the precipitates have the same size, this plot should be a straight line. This is obviously not the case here as one can fit a straight line only to the very narrow portion of the log I vs Q^2 curve (Figure 3) in the low Q region. (This is further ellustrated by Figure 7). Also, the absence of any peaks in the scattering curve indicates that particle density is low enough to neglect the interparticle interference $\Psi(Q)$ in Eq. 2. In the absence of ideal behavior, complex deconvolution schemes are required for obtaining the size distribution of the particles. Some attempts in this direction are described in the literature.

SANS characteristics of aged samples are shown in Figure 4. According to the theory of nucleation and growth, for an alloy of asymmetric composition, as one increases the temperature of aging the equilibrium volume fraction of the second phase decreases because the miscibility gap becomes narrower at high temperatures. However, as long as the reaction is controlled mainly by the interdiffusion coefficient, the volume fraction precipitated in the "same" time period will increase as the aging temperature increases*. This is very nicely indicated by Figure 4. Overall integrated intensity is lowest for #21 as this curve lies below the rest in the scattering pattern (Figure 4). Upon aging at 1000°F; there is a significant rise in the

---

* This behavior will be obeyed until the temperature is high enough to intersect the nose of the 'C' curve in the TTT diagram, above which temperature the reaction is driving force controlled instead of diffusion controlled.

intensity in the Q region 0.003 to 0.008nm^{-1}, signifying an increase in the volume fraction of the precipitates in the size range 80 to 20.0nm. With a further increase in the aging temperature to 1100°F, a cross-over appears between the scattering curves which move to lower Q values with continuing increases in the temperature (see specimens 22, 23, and 24). This signifies that due to more rapid diffusion at higher temperatures, enough "growth" and coarsening is taking place in 90 minutes that the size distribution is shifted to larger sizes and hence the scattering curve shifts to lower Q values.

Correlation of the aforementioned results with the hardness data is not direct. From Table 1, we can see that hardness is highest for #21 and it decreases as one ages isochronally at higher temperatures. According to the prevalent theories of precipitation hardening, there are two dislocation mechanisms which can control the strength of an age-hardened material. These are (1) dislocation cutting, and (2) dislocation bowing. If precipitates are softer than the matrix, then dislocations can easily cut through the second phase particles. It is therefore desirable that precipitate elastic constants be higher than the matrix. The bowing of dislocations can be prevented by obtaining a fine dispersion of the overall volume fraction of precipitates such that the inter-particle distance is minimum. If the inter-particle distance is low, then a higher shear stress is required to bow a dislocation through the precipitates. This action results in higher strength. Even though it is clear from Figure 4 that the volume fraction of copper precipitates present in sample #21 is lower than in the other samples, the distribution is finer. This results in a smaller interparticle spacing compared to the other samples. Therefore, a higher hardness is obtained. One conclusion which

becomes clear immediately in this case is that as hardness decreases (from #21 to #24), the scattered intensity in the high Q region increases, but in the low Q region, it decreases. This observation also points to a shift of precipitate size distribution to larger sizes.

Another interesting correlation is revealed when we plot total neutron cross-section (Table 1) versus the hardness values (Figure 5). As hardness increases, the total neutron cross-section decreases. This decrease is equivalent to the sample becoming more transparent to the neutron beam (or the sample transmission per unit thickness increasing). This observation is consistent with Figure 4 in the sense that the scattering curve for the sample with lowest total neutron cross-section lies underneath all the other curves (#21 in Figure 4). Such total cross-section increase with increasing aging temperature is indicative of the fact that the overall integrated SANS intensity, and therefore the volume fraction of the second phase, increases with an increase in aging temperature. The simplicity of the correlation between hardness and the total cross-section for the isochronally aged samples is rather striking and thus has some potential for being a good NDE tool.

Only sample numbers 14 and 22 provided for this study are from an isothermally aged lot. According to the theory of nucleation and growth and its correlation to SANS (see Figure 1), a translation of SANS curves with aging time is expected during the isothermal evolution. Figure 6 shows scattering curves for the A710 samples aged for 30 and 90 minutes respectively at 1000°F. We can see that due to the additional hour of aging, the scattered intensity increases over almost the entire Q range, except that a slight decrease is observed in the small portion of the high Q region. In

this case the hardness and total cross-section trend similar to the isochronally aged samples is followed. Sample #22, which is a strong scatterer compared to #14, also has a larger total cross-section, but a lower hardness (98.5 HRB vs 99.8 HRB) (see Table 1).

We have interpreted the translation of the SANS curves with the increase in aging temperature (figure 4) as a shift of precipitate size distribution to the higher sizes. In the absence of detailed size distribution analysis, this fact should also be reflected by the increase in Guinier radius with the aging temperature. Hence a "Guinier" analysis was carried out for the spectra of all samples. NBS program DATAPLOT was used for fitting Eq. (2) (with $\Psi(Q)=0$) to the relevant part of the SANS curves. An example of this fit is shown in Figure 7, with the blank squares indicating the data points and a continuous line as the fitted line. For sample #14, the radius of gyration or "Guinier" radius was 17.7nm, which translates to a particle size of 45.7nm. Radius of gyration for other samples is given by the last column of Table 1. It is our belief that all the R_G values marked by an asterik are unreliable. Let us look at Figure 4 and samples 21 to 24. There, the scattering curve translates towards the main beam. Under such a situation, not only do the resolution corrections become progressively large, but the real "Guinier region" also becomes inaccessible. Therefore in order to carry out appropriate Guinier analyses for samples 22, 23, 24, further measurements must be performed in the Q region much lower than the lowest ($0.001nm^{-1}$) covered in this study. This also suggests that samples heat treated at temperatures above 900°F have a large fraction of particles larger than 60nm in size.

Table 1. Test sample details

Sample Number	Aging Treatment	Hardness	Thickness Cm	Transmission at λ_n=6.2A	Total Neutron Cross Section (cm^{-1})	Guinier Radius RG(nm)
14	30min/1000°F	99.8R_B	0.293	0.76139	0.93041	17.707
21	90min/900°F	23.2R_C ~100.2R_B	0.291	0.77241	0.88742	17.97
22	90min/1000°F	98.5R_B	0.2909	0.75254	0.97732	16.64*
23	90min/1100°F	93.8R_B	0.2921	0.74691	0.99901	15.7*
24	90min/1200°F	89.0R_B	0.2995	0.73738	1.0172	16.44*

*Reliability of these R_G values is questionable. See the text for relevant explanation.

Table 2. SANS parameters for A710 Steel

Wavelength	-	6.2 A° ± ($\Delta\lambda/\lambda$~0.25)
Monochromator	-	Mechanical Velocity Selector
Source of Neutrons	-	10 MW Reactor
Filters	-	15" Be and 10" Bi Single Crystal
Detector Size	-	65X65 cm ∿ 110X110 active channels
Detector gas	-	^{3}He + Xe
Detector distance	-	3.6 meters
Beam Size	-	1.2 cm.
Collimation	-	iris 27mm - 12mm, 4.1 meters apart

Sample to entrance collimator distance 4.50 meters.

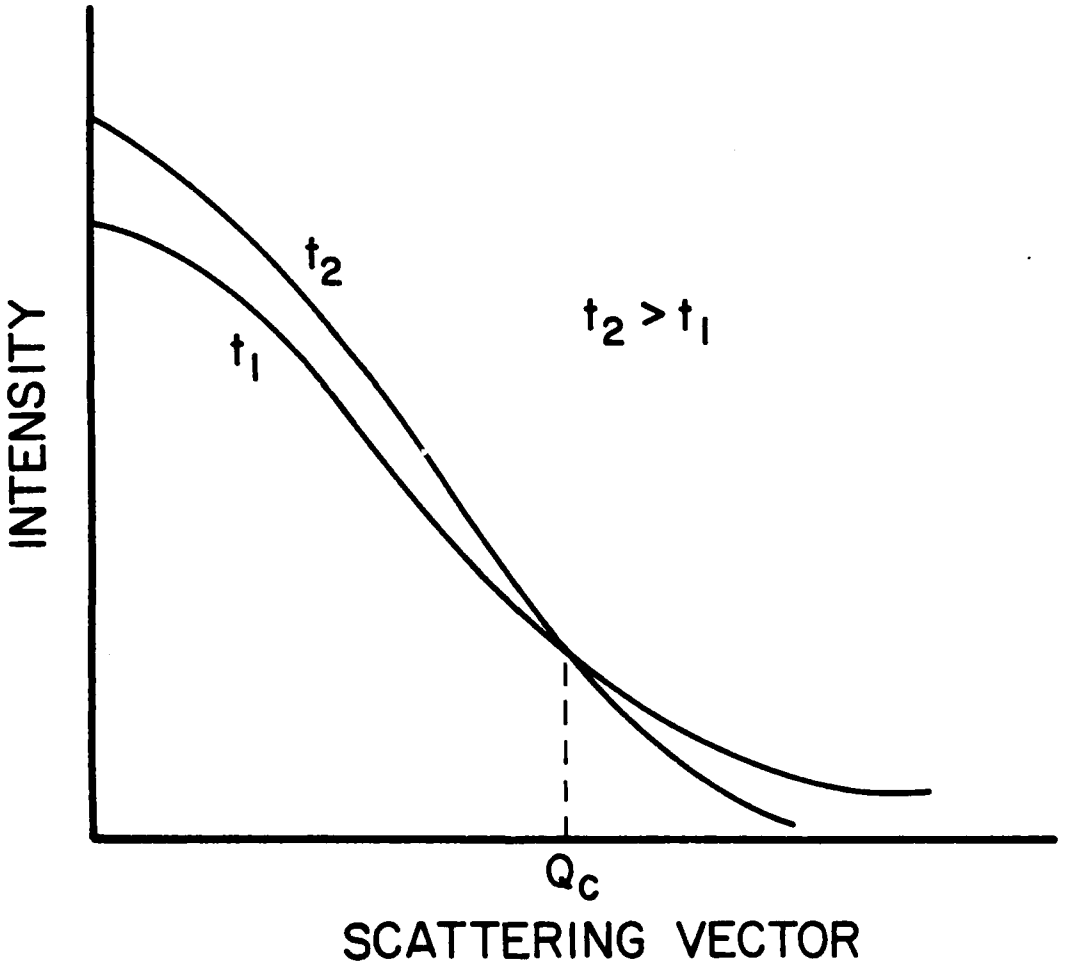

Figure 1. SANS results showing intensity versus scattering vector. t_1 and t_2 denote aging times at a fixed temperature.

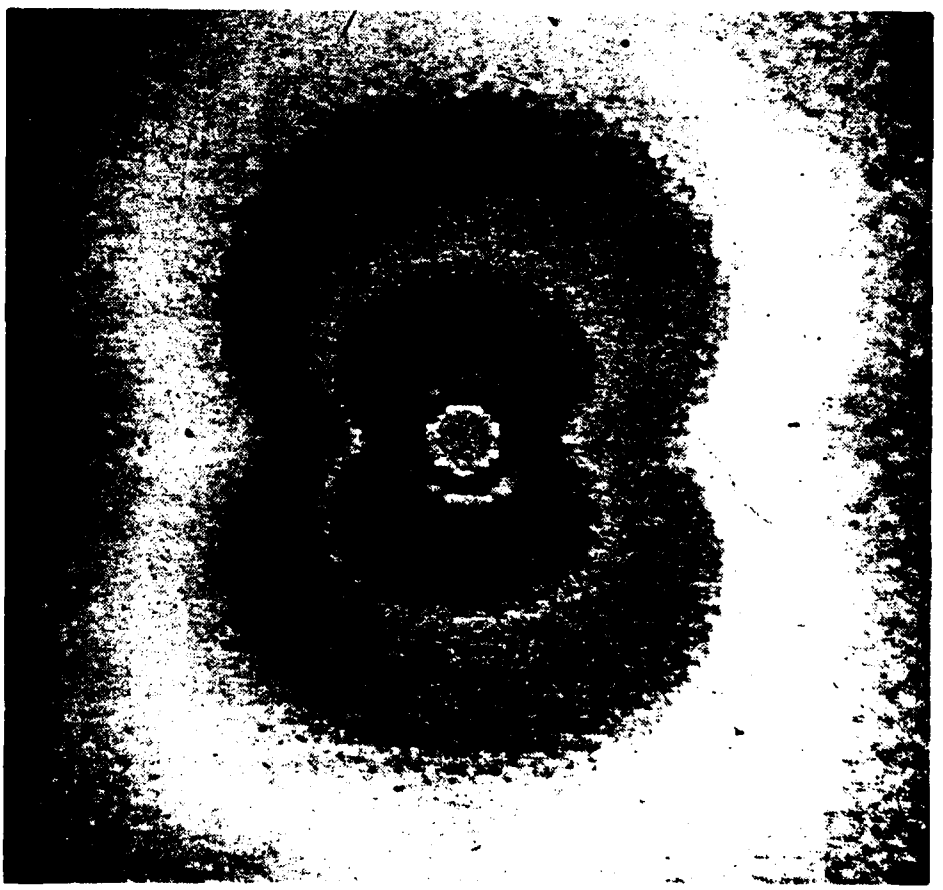

Figure 2. Two dimensional detector pattern for specimen number 23.

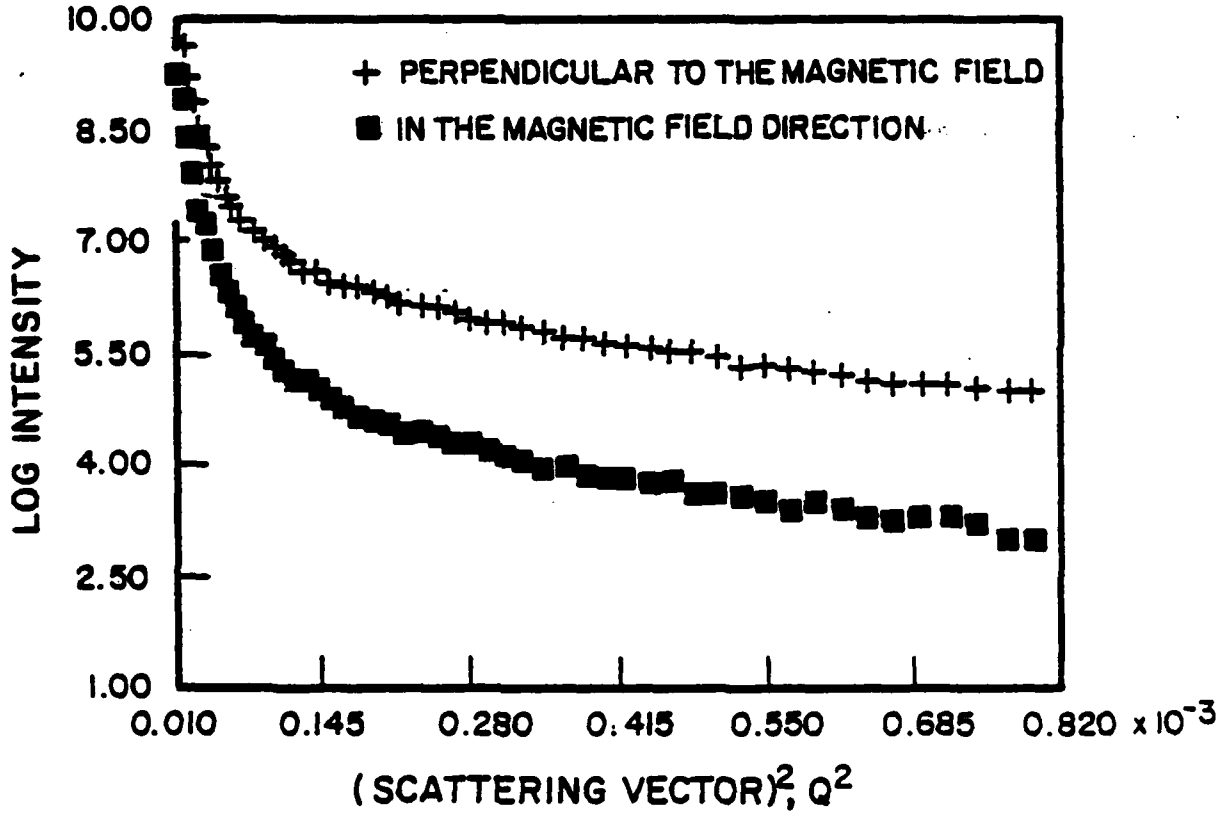

Figure 3. Guinier plot of log intensity versus the scattering vector squared.

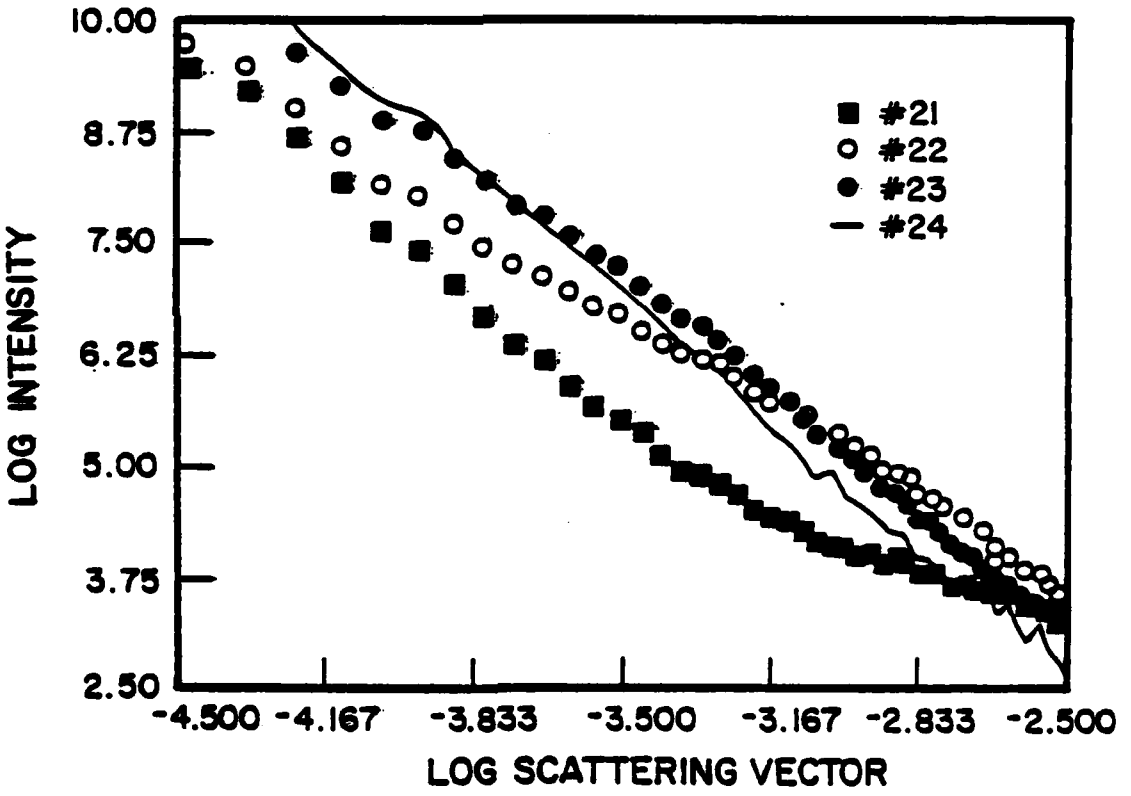

Figure 4. Log intensity versus log scattering vector for the isochronally heat treated (90 min) specimen. 21-900°F; 22-1000°F; 23-1100°F; and 24-1200°F.

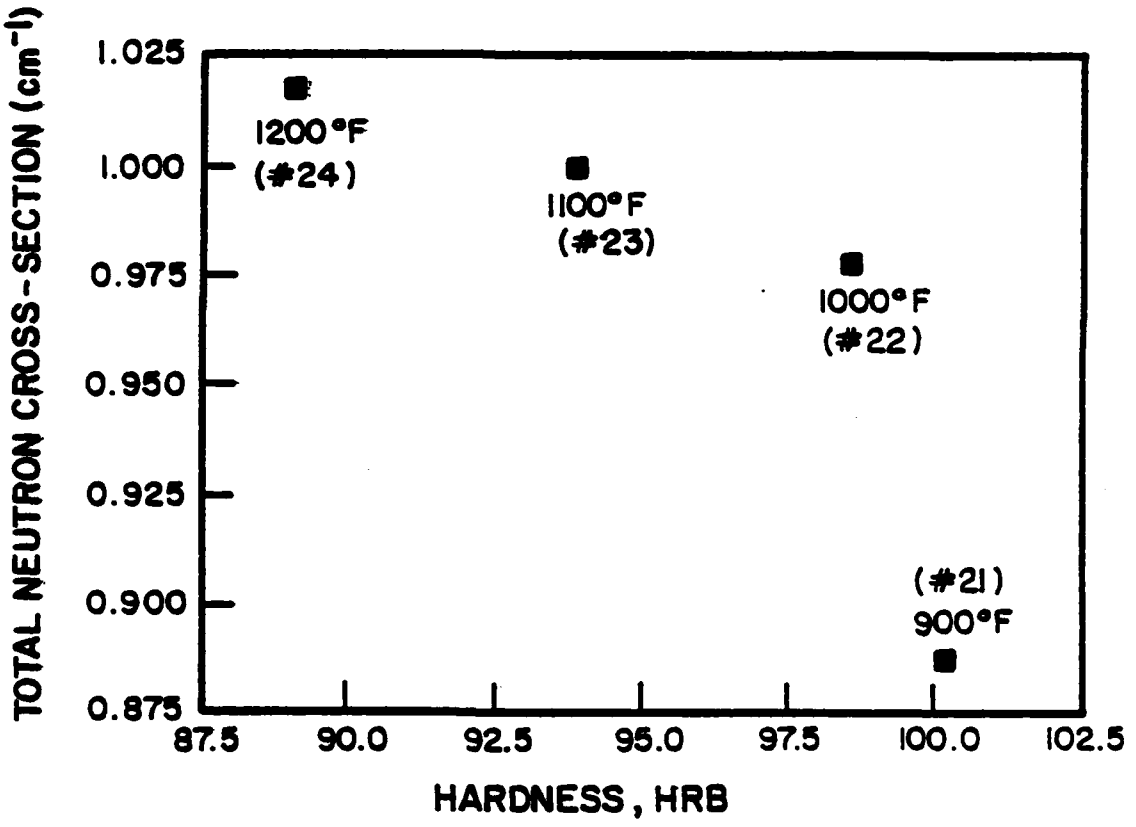

Figure 5. Total neutron cross-section versus hardness, HRB. Parenthesis indicate specimen identity.

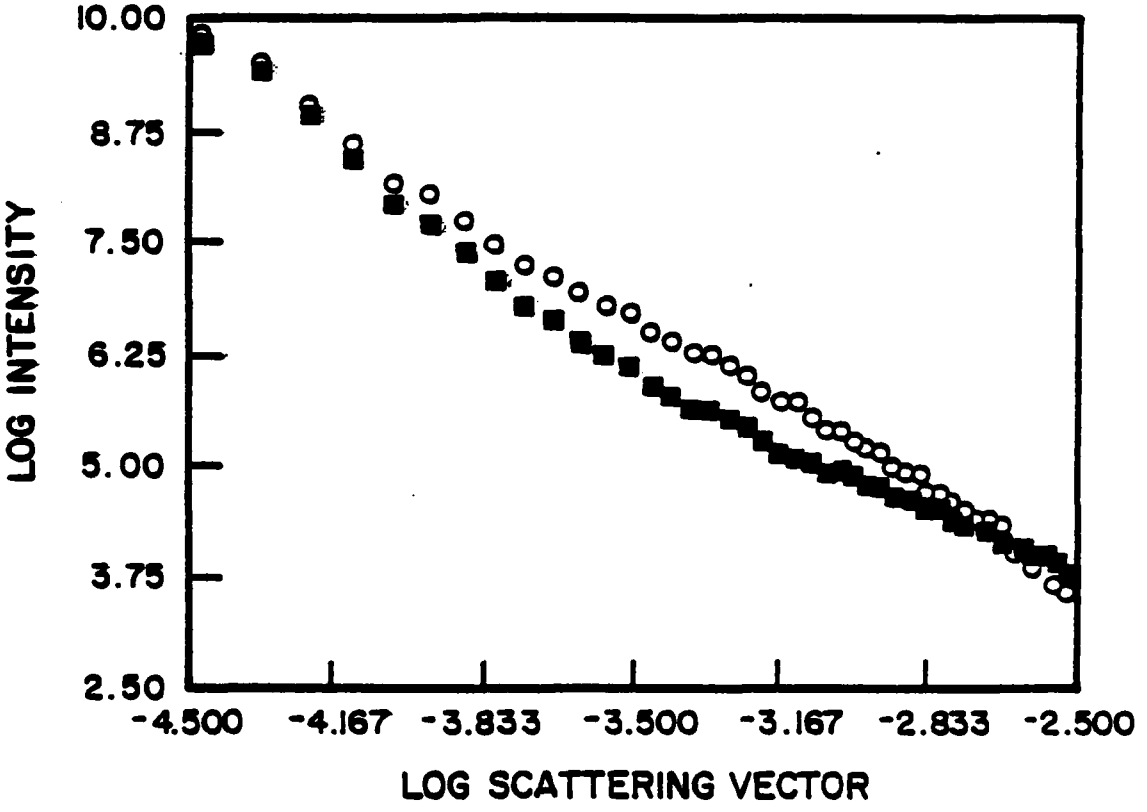

Figure 6. Log-log plot of intensity versus scattering vector for specimens #14 (30 min age at 1000°F) and #22 (90 min age at 1000°F).

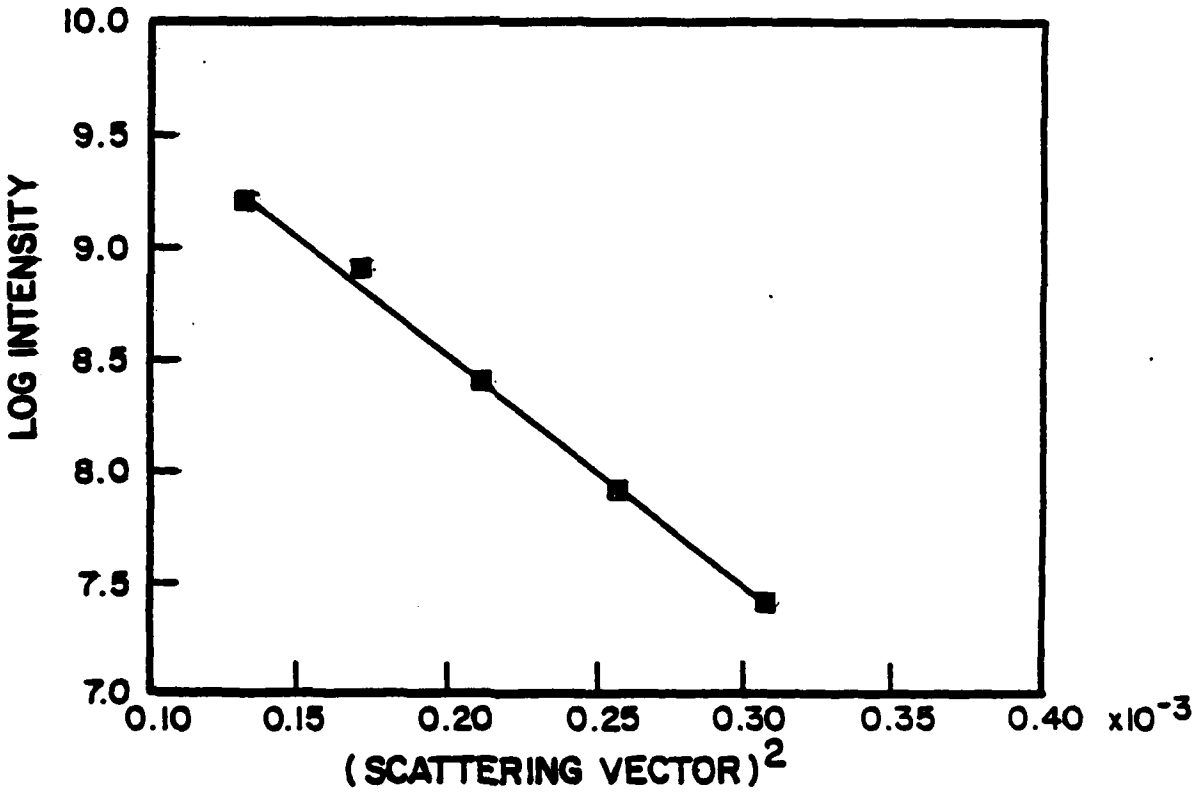

Figure 7. Log intensity versus scattering vector squared. Fit of Guinier function to the data for sample 14.

INITIAL DISTRIBUTION

Copies

14 NAVSEA

- 1 (SEA 05M)
- 2 (SEA 05M2)
- 1 (SEA 05MP)
- 1 (SEA 05R)
- 2 (SEA 05R25)
- 2 (SEA 55Y)
- 1 (SEA 55Y.12)
- 1 (SEA 55Y3)
- 1 (SEA 08)
- 1 (PMS 400C)
- 1 (PMS 400D)

12 DTIC

CENTER DISTRIBUTION

Copies	Code
1	1101.2
1	1103
1	1104
1	17
1	1703
1	172
1	1720.4
1	173
1	173.2
1	173.6
1	1740.3
1	28
2	2803
1	2809
2	281
2	2812
20	2814
2	2815
2	2816
5	522.1
2	5231

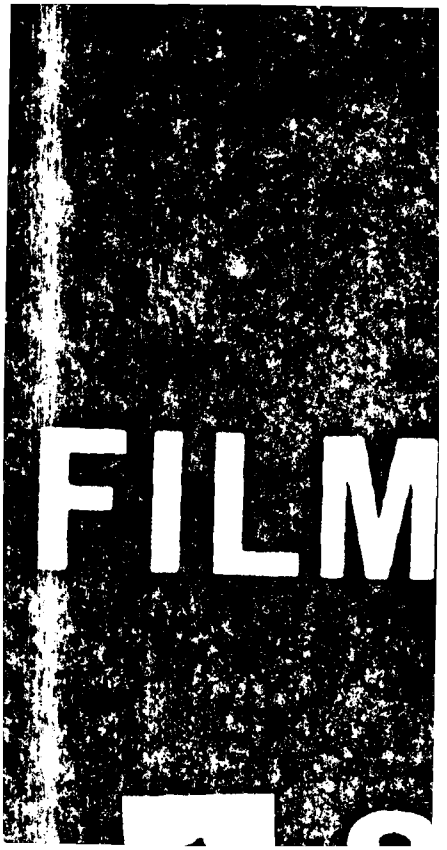
FILM